

UNLIMITED
DISTRIBUTION
ILLIMITEE

Communications Research Centre

HF DIRECTION FINDING BY WAVEFRONT TESTING

by

D.W. Rice

This work was sponsored by the Department of National Defence, Research and Development Branch
under Project No. 33G00.

CRC REPORT NO. 1333

DEPARTMENT OF COMMUNICATIONS
MINISTÈRE DES COMMUNICATIONS

TK
5102.5
C673e
#1333

IC

OTTAWA, MARCH 1980

COMMUNICATIONS RESEARCH CENTRE

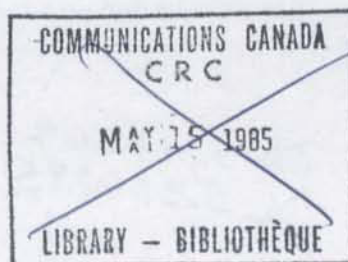
DEPARTMENT OF COMMUNICATIONS
CANADA

HF DIRECTION FINDING BY WAVEFRONT TESTING

by

D.W. Rice

(Radio and Radar Research Branch)



CRC REPORT NO. 1333

March 1980

OTTAWA

This work was sponsored by the Department of National Defence, Research and Development Branch under Project No. 33G00

CAUTION

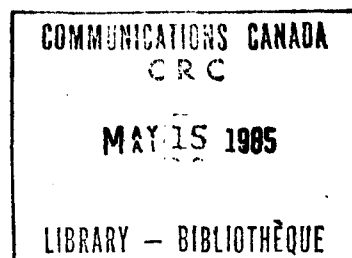
The use of this information is permitted subject to recognition of
proprietary and patent rights.

TK
5102.5
C673e
#1333
c.b

DD 5316369
DL 5316385

TABLE OF CONTENTS

ABSTRACT	1
1. INTRODUCTION	2
2. THE THREE-RAY RAYLEIGH-FADING PROBLEM	2
3. THE TWO-RAY PROBLEM	5
3.1 Probability Density and Distribution Functions	5
3.2 Wave-Front Non-Linearities	6
4. THREE-RAY INTERFERENCE	7
5. COMPARISON WITH EXPERIMENT	9
5.1 Interferometer Measurements, Mid-Latitude Path	9
5.2 Filled Aperture Measurements, Auroral Zone Path	11
5.3 Time Scales of Phase-Front Nonlinearities	11
5.4 Angle-of-Arrival Comparisons	12
6. CONCLUDING REMARKS	14
7. ACKNOWLEDGEMENT	14
8. REFERENCES	15
APPENDIX A - Mathematical Details	31
APPENDIX B - The Cumulative Probability Distribution for the RMS Phase Deviation in the Presence of Three Rays	41



HF DIRECTION FINDING BY WAVEFRONT TESTING

by

D.W. Rice

ABSTRACT

Calculations are reported of the probability of observation of various degrees of phase-front non-linearity, for two and three signals incident from different directions upon a phase-measuring array. It is assumed that the signals fade independently, and that their amplitude probability densities are described by a Rayleigh law. It is shown that, under the worst-case conditions of equal powers in the signals, the probability of observing an rms phase deviation of 25 degrees or less from the best-fit straight line to the phase along an array, is about 0.5 when 2 rays are present, and about 0.2 when 3 rays are present.

Experimental measurements over a 911-km mid-latitude path and a 2100-km trans-auroral-zone path, confirm the general behavior predicted by the theory. It is well known that amplitude fading can be attributed to various ionospheric effects; however the measurements show that modulation imposed on the signal at the transmitter can also play an important part in decorrelating the amplitudes of signals received (after different time delays) via different ionospheric modes. In the latter case, the modulation can markedly reduce both the waiting time between phase-linear events, and their duration.

The experimental program included concurrent measurements over the same path using FMCW, CW and SSB signals from a co-operative transmitter. The FMCW signals were processed to provide direction-of-arrival statistics on a mode-separated basis. The standard deviation of the direction-of-arrival varied from 0.3 degrees for E-mode signals, to 1.4 degrees for F2 high-angle signals. The CW and SSB signals were processed by selecting only those phase fronts with rms phase deviations of 10 degrees or less. For these, direction-of-arrival standard deviations were in the range 0.6 to 0.9 degrees, with slightly smaller deviations being observed for the CW signals.

1. INTRODUCTION

Wave interference arising from multiple propagation modes constitutes a significant source of error in HF direction-finding, particularly for those systems with apertures of a few wavelengths or less. One possible way to mitigate this effect is to take bearing measurements only at times when propagation appears to be nearly unimodal (i.e. dominated by one ionospheric mode). Probably the earliest attempt to do this was the "Dot-Lock" technique¹, in which bearings were taken on the leading edge of an amplitude-keyed signal. This technique was later extended to other types of modulation². Workers have also noted that it may be possible to take advantage of mode amplitude fading or scintillation, which provides periods of a basically plane-wave condition at the receiving array^{2,3}.

The time domain behavior of wave-front non-linearities observed at the Communications Research Centre with a 6-element linear interferometer of 663 metres total aperture has been reported earlier⁴. It was found that the rms deviation from a linear fit of the radio-wave phase across the receiving array varied slowly when an unmodulated CW signal was being received, and the time scale of the observed variations was commensurate with that reported for ionospheric channel fading rates⁵. On the other hand, when the transmitted signal was SSB-modulated, the time scale of changes in wave-front nonlinearity was commensurate with that of the modulation.

The foregoing work suggests that a simple phase linearity test is sufficient to select those bearing measurements which are relatively free of wave-interference error. While a scheme involving both phase and amplitude measurements might be more reliable⁶, good results were achieved without the additional complication of amplitude measurements. Further, it was found that, while the fading characteristics of the ionospheric channel provide periods in which one mode dominates, any amplitude modulation which may have been imposed on the signal at the transmitter also plays a part and, in particular, can markedly shorten the waiting time between phase-linear events.

In this paper we report an analysis of the three-ray Rayleigh-fading problem, of which the two-ray problem is a special case. Results are presented in terms of the probability of observation, across an antenna aperture, of an rms phase deviation less than some threshold value, as a function of that threshold. The theoretical results are compared with a more extensive set of measurements taken during the course of the experiment reported earlier⁴, and with some measurements made on another path which traversed the auroral zone.

In the main body of this report, the more mathematical results are given in outline form only. More detailed derivations may be found in Appendix A.

2. THE THREE-RAY RAYLEIGH-FADING PROBLEM

Let there be three rays with statistically-independent, Rayleigh-distributed amplitudes x_i , and with rms amplitudes $\sqrt{2}a_i$, $i=1,2,3$. Then the probability density functions are

$$f_{X_i}(x_i) = \frac{x_i}{a_i^2} \exp \left\{ -\frac{x_i^2}{2a_i^2} \right\}, \quad 0 \leq x_i < \infty; \quad i = 1, 2, 3 \quad (1)$$

We may reduce the dimensionality of the problem by normalizing the amplitudes with respect to x_1 , and then computing a two-dimensional probability density function by means of the theory of functions of random vectors⁸.

Define a 3-dimensional random vector

$$X = (X_1, X_2, X_3) \quad (2)$$

where the X_i , $i = 1, 2, 3$ are Rayleigh-distributed as given by equation (1).

Define a new random vector

$$Y = (Y_1, Y_2, Y_3) \quad (3)$$

where

$$\left. \begin{aligned} Y_1 &= X_1 \\ Y_2 &= \frac{X_2}{X_1} \\ Y_3 &= \frac{X_3}{X_1} \end{aligned} \right\} \quad (4)$$

The inverse of the transformation in equation (4) is

$$\left. \begin{aligned} X_1 &= Y_1 \\ X_2 &= Y_1 Y_2 \\ X_3 &= Y_1 Y_3 \end{aligned} \right\} \quad (5)$$

Hence, using the assumption that the X_i are statistically independent, the joint probability density for the Y_i is

$$f_{Y_1 Y_2 Y_3}(y_1, y_2, y_3) = J f_{X_1}(y_1) f_{X_2}(y_1 y_2) f_{X_3}(y_1 y_3) \quad (6)$$

where J is the Jacobian of the inverse transformation in equation (5),

$$J = \begin{vmatrix} \frac{\partial x_1}{\partial y_1} & \frac{\partial x_1}{\partial y_2} & \frac{\partial x_1}{\partial y_3} \\ \frac{\partial x_2}{\partial y_1} & \frac{\partial x_2}{\partial y_2} & \frac{\partial x_2}{\partial y_3} \\ \frac{\partial x_3}{\partial y_1} & \frac{\partial x_3}{\partial y_2} & \frac{\partial x_3}{\partial y_3} \end{vmatrix} = y_1^2 \quad (7)$$

Combining equations (7), (6) and (1) yields

$$f_{Y_1 Y_2 Y_3}(y_1, y_2, y_3) = \frac{y_1^5 y_2 y_3}{a_1^2 a_2^2 a_3^2} \exp - \left\{ \frac{y_1^2}{2a_1^2} + \frac{y_1^2 y_2^2}{2a_2^2} + \frac{y_1^2 y_3^2}{2a_3^2} \right\} \quad (8)$$

The joint probability density for variables y_2 and y_3 is obtained by integrating equation (8) over y_1 ,

$$f_{Y_2 Y_3}(y_2, y_3) = \int_0^{\infty} f_{Y_1 Y_2 Y_3}(y_1, y_2, y_3) dy_1$$

which after some algebra yields

$$f_{Y_2 Y_3}(y_2, y_3) = \frac{8(y_2/b_2^2)(y_3/b_3^2)}{[1 + (y_2/b_2)^2 + (y_3/b_3)^2]^3}, \quad 0 \leq y_2 < \infty; \quad 0 \leq y_3 < \infty \quad (9)$$

where $b_2^2 = a_2^2/a_1^2$ and $b_3^2 = a_3^2/a_1^2$ are the mean powers in rays 2 and 3 respectively, normalized to ray 1. It is readily shown from equation (9) that the probability density function $f_{Y_2 Y_3}(y_2, y_3)$ has a maximum at $(\frac{1}{2}b_2, \frac{1}{2}b_3)$, where its value is $16/(27b_2b_3)$.

As an illustrative example, the two-dimensional probability density function of equation (9) is shown in contour form in Figure 1, for arbitrary parameter values $b_2 = 1.5$ and $b_3 = 2.0$.

3. THE TWO-RAY PROBLEM

We digress here to consider the two-ray problem, since it serves as a useful introduction to the continuation of the three-ray problem which will follow.

3.1 PROBABILITY DENSITY AND DISTRIBUTION FUNCTIONS

The marginal probability density of variable y_2 may be obtained by integration of equation (9) over y_3 , which yields

$$f_{Y_2}(y_2) = \frac{2 y_2}{b_2^2(1 + y_2^2/b_2^2)^2}, \quad 0 \leq y_2 < \infty \quad (10)$$

which is just the probability density function for the two-ray case⁷.

The probability that the variable Y_2 is less than or equal to the value y_2 , that is, the cumulative probability distribution function for y_2 , is

$$F_{Y_2}(y_2) = \int_0^{y_2} f_{Y_2}(y_2) dy_2 = 1 - \frac{b_2^2}{b_2^2 + y_2^2}, \quad 0 \leq y_2 < \infty \quad (11)$$

It is more convenient, since either ray may dominate, to define a new variable r on the range $\{0,1\}$, such that

$$r = \begin{cases} y_2, & 0 < y_2 \leq 1 \\ 1/y_2, & 1 < y_2 < \infty \end{cases} \quad (12)$$

The variable r is the ratio of the amplitude of the weaker ray to that of the stronger ray, regardless of which one dominates. The cumulative probability distribution for r is then

$$F_R(r) = P[R \leq r] = F_{Y_2}(r) + 1 - F_{Y_2}\left(\frac{1}{r}\right)$$

or

$$F_R(r) = 1 + \frac{r^2 b_2^2}{1 + r^2 b_2^2} - \frac{b_2^2}{b_2^2 + r^2}, \quad 0 \leq r \leq 1 \quad (13)$$

This result will be required in the next sub-section.

3.2 WAVE-FRONT NON-LINEARITIES

Two-ray interference is most easily visualized as the weaker ray producing corrugations in the otherwise plane equi-phase surface associated with the stronger ray⁹. It can be readily shown¹⁰ that the deviation ϕ from the phase of the stronger wave is given by

$$\tan \phi = \frac{r \sin \theta}{1 + r \cos \theta} \quad (14)$$

where r is the ratio of ray amplitudes as defined in equation (12), and θ is given by

$$\theta = kx(\cos \psi_1 - \cos \psi_2) - \omega_d t \quad (15)$$

Here k is the wave number ($2\pi/\text{wavelength}$), x is the distance along the array, ψ_1 and ψ_2 are the angles between the ray directions and the array axis, ω_d is the radian frequency difference between the two signals (due, for example, to Doppler shifts), and t is the time.

The mean-square phase deviation across a large antenna aperture is given by

$$\sigma_\phi^2(r) = \frac{1}{2\pi} \int_0^{2\pi} \phi^2(r, \theta) d\theta \quad (16)$$

where ϕ is given by equation (14). The result of a numerical evaluation of equation (16) has been reported earlier⁴, where it was shown that $\sigma_\phi(r)$ is an approximately linear function of r . This relationship is also shown here in Figure 2. The integration over 2π in θ is equivalent to spatial integration over one period of the interference pattern, and hence is the result applicable when the antenna aperture is large compared to one period of the interference pattern. If the aperture is smaller than the period of an interference pattern, then the observed mean square phase deviation will be smaller.

The numerical result shown in Figure 2 may be combined with the cumulative distribution function of equation (13) to yield the cumulative distribution function for the rms phase deviation. This result is shown in Figure 3. Note that for the worst case, when the mean powers in the two rays are equal, the probability that an rms phase deviation of less than 25° will be observed is approximately 0.5.

Figure 2 shows that the rms phase deviation σ_ϕ is an approximately linear function of the ray amplitude ratio r . Thus σ_ϕ should exhibit the same statistics as r . If a CW signal is transmitted, the time-domain behavior of the rms phase deviation σ_ϕ should then correspond to that of the ionospheric channel. On the other hand, if there are rapid amplitude variations because of signal modulation, then r may be thought of as the ratio of the magnitudes of the modulation envelopes as transmitted via the

two ionospheric modes, with the weaker signal a time-shifted and amplitude-scaled version of the other. In this case, provided the time delay is at least of the order of the reciprocal of the modulation bandwidth, the time-domain behavior of the ratio r , and therefore the rms phase deviation σ_ϕ , depends primarily on the modulation, with a slow-varying ionospheric component superimposed.

4. THREE-RAY INTERFERENCE

When 3 rays are present, it is possible that the sum of the amplitudes of any two rays may exceed that of the third. There is then no ray which dominates, and the associated wave-fronts become highly irregular in shape, with large deviations from linearity. This condition we refer to as "strong" wave interference. The probability of occurrence of this strong interference, may be obtained by integrating the density function of equation (9) over the appropriate region in (y_2, y_3) space. The boundaries for the integration are illustrated in Figure 4. The regions labelled 1, 2, and 3 are those in which rays 1, 2, and 3 respectively may be considered to dominate, a condition we refer to as "weak" wave interference. It is shown in Appendix A that the integral of equation (9) over the region of strong wave interference of Figure 4 yields

$$P[S] = \frac{\pi b_2 b_3}{(1+b_2^2+b_3^2)^{3/2}} \quad (17)$$

where $P[S]$ denotes probability of strong interference, and b_2^2 and b_3^2 are the ratios of the mean powers in rays 2 and 3 respectively, normalized to ray 1, as previously defined following equation (9). Figure 5 shows contours of $P[S]$ in (b_2, b_3) co-ordinates. The maximum probability of strong interference is 0.605, occurring when the mean powers in all three rays are equal. Thus in the worst case there is still an approximately 40% probability that one of the three rays will dominate, that is, its amplitude will be greater than the sum of the other two.

As in the 2-ray case, in order to compute cumulative probability distributions for the rms phase deviation across an antenna aperture, it is necessary to resort to numerical methods. This computation involves integration of the probability density function of equation (9) over regions of (y_2, y_3) space defined by contours of constant rms phase deviation. Such contours can be fairly readily calculated in the regions of weak wave interference, where the result is not greatly affected by the arbitrary relative starting phases of the signals representing the 3 rays. Some contours of constant rms phase deviation σ_ϕ are shown plotted in Figure 6. The probability density function (equation (9)) which is integrated over regions defined by these contours is a function of b_2^2 and b_3^2 , although the contours themselves are not.

In the region near the origin in Figure 6, the contours of constant rms phase deviation are closely approximated by quarter-circles. This means

that the rms deviation of the phase from that of the strongest ray is a function of the total power in the other two rays, regardless of how it is distributed between them. This relationship is shown in Figure 7.

In order to calculate the probability that an rms phase deviation will be less than one of the circular contours in Figure 6, it is convenient to change to polar co-ordinates in equation (9). Thus, with the substitutions $y_2 = z \cos\theta$, $y_3 = z \sin\theta$, the integral of equation (9) out to radius z is given by

$$P[Z \leq z] = \int_{z=0}^z \int_{\theta=0}^{\frac{\pi}{2}} \frac{8 b_2^4 b_3^4 z^3 \sin\theta \cos\theta}{[b_2^2 b_3^2 + z^2 (b_3^2 \cos^2\theta + b_2^2 \sin^2\theta)]^3} d\theta dz \quad (18)$$

which can be evaluated to yield

$$P[Z \leq z] = 1 - \frac{b_2^2 b_3^2 + (b_2^2 + b_3^2) z^2}{(b_2^2 + z^2)(b_3^2 + z^2)} \quad (19)$$

where $z^2 = y_2^2 + y_3^2$. In the region $z^2 < 1$, equation (19) gives the probability

that ray 1 dominates by the factor $z = \frac{(x_2^2 + x_3^2)^{\frac{1}{2}}}{x_1}$, where the x_1 are the

amplitudes associated with the three rays. The probability that ray 2 or ray 3 dominates can in principle be computed by integrating over the relevant regions of the probability density function; however it is easier to permute suitably the ray amplitudes and make repeated use of equation (19).

Combining the results of equation (19) and Figure 7, one may compute the probability that any ray dominates sufficiently to produce an rms phase deviation less than some threshold, as a function of that threshold. The range of validity encompasses thresholds between 0° and 32° , where the contours of constant rms phase deviation are circular, as illustrated in Figure 6. For rms phase deviations larger than 32° , a different procedure must be used because the rms phase deviation becomes a much stronger function of the relative starting phases associated with the different rays. This is illustrated in Figure 8, which shows the relative phase across a 16.6-wave-length aperture, for ray amplitudes of 1.0, 0.75, and 0.27, and various relative starting phases.

Appendix B outlines a method of obtaining the probability distribution for the rms phase deviation, without the restriction to small deviation values. This method was used to confirm the result above for small thresholds, as well as to extend the result to include all possible threshold values. Some results are shown in Figure 9. Curve 1 is the result when the average powers in the three rays are equal, while curve 2 is for the case in which the mean powers in rays 2 and 3 are equal, and sum to $1/4$ the power in the strongest ray. For comparison, curves 3 and 4 show similar results for the 2-ray case which was illustrated earlier in Figure 3.

The rms phase deviation has an upper limit of 52° * when only two rays are present. The upper limit for 3 rays is less definite, but for practical purposes appears to be about 125° .

It was noted earlier in connection with Figure 3, that there is an approximately 50% probability of observing an rms phase deviation of 25° or less, when two rays with equal average powers are present. From Figure 9, it may be noted that this probability drops to about 0.2 when three rays of equal average powers are present.

5. COMPARISON WITH EXPERIMENT

There are two main points of difference between the idealizations assumed in the earlier theoretical discussion and calculations, and any measurements which can be made. The first is that the calculations assumed a very large antenna array, that is, one in which the angular separation of incoming rays was much greater than the array beamwidth. On the other hand a likely application of wave-front testing is to the situation in which the ray separation is of the order of a beamwidth or less. A second difference is that it may be desirable to use a very sparse array, rather than the filled (or continuous) aperture assumed for the calculations. Both of these factors would cause the measured rms phase deviations to be smaller than the calculations predict.

A secondary consideration is that the calculations neglect the effect of noise. For good signal-to-noise ratios, the measurable effect is to reduce the occurrence of very low rms phase deviations. This can be seen in the experimental results which follow, for rms phase deviations of less than 10° or so.

5.1 INTERFEROMETER MEASUREMENTS, MID-LATITUDE PATH

As reported earlier⁴, some measurements have been made over a 911 km path between Sept Iles, Quebec and Ottawa, Ontario, in which the receiving array at Ottawa contained 6 elements over a total aperture of 662.9 metres. (The array and associated instrumentation were part of the HF Direction-Finding Research Facility at the Communications Research Centre¹¹.) Inter-element spacings of 15.2, 30.5, 68.6, 167.6 and 381.0 metres were used, and the axis of the array was aligned in a direction perpendicular to the propagation path. Each of the six elements in the array was connected to a separate, phase-stable receiver with quadrature product-detector outputs. Each receiver output was sampled and digitized at a rate of 1638.4 samples/second for the SSB and CW signals, and at a rate of 128 samples/second for the FMCW signals.

The transmitted signals consisted of a sequence of FMCW, CW, and SSB which was repeated every two minutes. Figure 10 shows the timing of the sequence, while Table 1 gives the relevant parameters. The two-minute repetition interval of the sequence was interrupted every 20 minutes to make

* The rms of a uniform density between -90 and $+90$ degrees is 52° .

an oblique sounding over the same path. The frequency of operation was between 7.5 and 8.0 MHz, except for a two hour period in the early morning of the second day, when it was 5.3 MHz. The frequency was chosen on the basis of the oblique ionogram information to maximize the range of mode delays present over the path.

TABLE 1
Transmitted Signal Parameters

FMCW	
sweep rate	25 KHz/sec
sweep duration	4 seconds
3 dB range resolution after processing	15 μ seconds
CW	
duration	5 sec
3 dB Doppler resolution	0.3 Hz
SSB	
duration	5 sec
pseudo — random modulation, repeat period	64 msec
bandwidth	800 Hz
All signals	
transmitted power	50-100 watts

The measurements reported here were made on two consecutive days, on June 16, 1977 between 0900 and 2100 Eastern Standard Time, and on June 17 between 0425 and 1700.

Figures 11 and 12 show cumulative distributions of occurrence as a function of rms phase-deviation threshold for wave-front nonlinearities as measured by the six-element interferometer. The points denoted by the symbol + indicate data from the CW portion of the signal, while the points denoted by the symbol o indicate the results for the SSB portion of the signal. The solid line is a theoretical curve (as in Figure 3), based on the assumption of two rays present, and adjusted for reasonable fit to the data through the parameter b^2 which is the ratio of mean powers in the two rays. The theoretical curves in Figures 11 and 12 are intended only to illustrate that the measured distributions have a shape similar to that which would be expected theoretically. It is unlikely that the ratio of mean powers in the two strongest rays was as small as that indicated. It is more likely that the distributions have been somewhat shifted to the left as a result of the two factors mentioned earlier: the small angular separation of the incoming rays, relative to the array beamwidth, and secondly the sparseness of elements within the array.

It was known from the FMCW sounding data that there were four or five modes propagating most of the time. It would seem from the results of Figure 11 and 12, that only the two strongest modes were significant with

respect to the wave-front test. There was no evidence of strong wave interference as defined in the earlier discussion of the three-ray case.

It may be noted from Figures 11 and 12 that the occurrence of phase front non-linearities was slightly higher for the SSB signal than for the CW signal. This may be due, at least in part, to the signal processing which was slightly different for the two signals. The CW data was digitally filtered to reduce the noise bandwidth by a factor of about 4, and to eliminate spurious dc offset in the receiver outputs. This additional processing could not be done for the SSB signal because of its wider bandwidth.

5.2 FILLED APERTURE MEASUREMENTS, AURORAL ZONE PATH

In another experiment using the CRC facility, measurements were made over a 2100 km north-south path between Frobisher Bay and Ottawa. Data were recorded from 42 element locations within the larger, 1181 metre aperture, and from 16 locations within the 236 metre orthogonal aperture. The direction to the transmitter was 5.4° from the bisector of the two arrays. Fixed-frequency transmissions of five seconds duration were made once per minute, with gaps every 20 minutes when oblique ionograms were produced.

Figure 13 shows measured cumulative probability distributions of rms phase deviation for both arrays obtained over an approximately 6 hour period, and, for the longer array, a subset of these data for a 35 minute time period. The data from the longer array are similar in magnitude to the results derived earlier for the 3-ray case. On the other hand, the shorter aperture is not able to measure the full extent of phase front deviations, and the result appears to agree more closely with the theoretical two-ray curves.

5.3 TIME SCALES OF PHASE-FRONT NONLINEARITIES

As reported earlier⁴, the time scale of variations in phase-front shape can extend over a wide range of values. This point can be demonstrated from the time-domain behavior of the rms phase deviation as observed in the interferometer experiment described in Section 5.1. An example of the variation of the measured rms phase deviation, over a 5-second period, is shown in Figure 14 for a CW signal. The rms deviation changes with a time scale of the order of one second, a value commensurate with the rate to be expected for ionospheric channel fading⁵. The normalized auto-covariance function (correlation coefficient) for the data of Figure 14 is shown in Figure 15. The covariance function has the general appearance of a decaying cosine, with the first zero crossing at 1.7 seconds. This means that low values of rms deviation, corresponding to the dominance of one ray, should persist, once present, for a few hundred milliseconds or more. Conversely, if one is observing a high rms phase deviation, it probably will be necessary to wait a similar length of time for a quasi-single-moded condition to reappear.

It should be noted that in cases in which the period of the interference pattern is larger than the array aperture, another source of significant time variation in the observed rms phase deviation is the drift of the interference pattern across the array. Drift of the interference

pattern is a manifestation of differential Doppler shift between rays. While the issue is not crucial to the conclusions reached here, other observations¹⁰ do support the view that, for mid-latitude circuits and apertures of the size used here, ray amplitude fading is the dominant cause of phase front decorrelation, although undoubtedly drifts due to differential Doppler shifts also contribute.

The time variation of the rms deviation σ_ϕ for the modulated portion of the signal is shown in Figure 16. The result is in sharp contrast to that shown in Figure 14 for a CW signal. Note in particular that low values of rms deviation recur much more frequently for the modulated signal, but they do not persist. The normalized auto-covariance function for the data of Figure 16 is shown in Figure 17. The correlation is small almost everywhere, except for impulses recurring at multiples of the basic period (64 milliseconds) of the pseudo-random sequence used as the modulating signal. (The impulse at zero delay is obscured by the y-axis.) The magnitude of the impulses dies away at longer times, corresponding to the decorrelation produced by the ionospheric channel, as shown in Figure 15.

As a summary of the entire 12 hours of measurements on the first day of the 2-day trial, the normalized auto-covariance function obtained by averaging the corresponding power spectra for the CW data is shown in Figure 18, while Figure 19 shows the corresponding auto-covariance function for the data from the modulated signal. Again, the marked difference in time scale between the two cases clearly illustrates that modulation can markedly influence such observations.

5.4 ANGLE-OF-ARRIVAL COMPARISONS

The objective in applying a wave-front test is to improve the accuracy of DF measurements. Applied to an interferometer array such as that used here, wave-front testing is an attractive way of making available the benefits of a rather large aperture at the expense of only a small number of antenna elements.

A pertinent question is the DF performance of an interferometer which uses a wave-front test. The experimental work accomplished to date and reported in earlier sections of this paper was not optimum to answer this question because only a single linear array was used. Measurements using two orthogonal arrays offer the potential benefit of sorting by elevation angle, so that performance in that case could approach that available via the mode which provides the best angular accuracy. Without elevation-angle sorting, the variance in measured bearing should, at best, lie somewhere between the intrinsic accuracy provided by each of the modes considered in isolation.

The FMCW data collected in the interferometer experiment were computer-processed to provide angle-of-arrival standard deviation statistics for each of the modes which could be isolated by virtue of their separation in time delay. The bearing has been taken as equal to the incidence angle measured with respect to the array axis, since the transmitter was located in a direction broadside to the array. Table 2 shows the average standard deviation of the bearing for each mode for each of the two days, each standard deviation contributing to the average being based on a 1-hour measurement interval.

Standard deviations range from about .3 degrees for the E mode, up to 1.36 degrees for the F2(o)H mode (F2 layer, ordinary magnetoionic component, high angle ray).

TABLE 2

Standard Deviation of Bearings, Classified by Ionospheric Mode, Range-Resolved FMCW Data

Mode of Propagation	Standard Deviation, Degrees	
	Day 167	Day 168
EL	.33	.40
EH	.27	*
E _s	.67	*
F1(o)L	1.18	.93
F1(o)H	1.05	.84
F1(x)H	*	.86
F2(o)L	1.07	*
F2(o)H	1.36	*

* Insufficient Observations

Key to mode designations:

E ionospheric E layer
 E_s sporadic E
 F1 ionospheric F1 layer
 F2 ionospheric F2 layer
 L low-angle ray
 H high-angle ray
 (o) ordinary magnetoionic component
 (x) extraordinary magnetoionic component

Table 3 shows the result of a similar analysis performed on the CW- and SSB-signal data. A bearing was derived from the average of all those phase-front measurements which passed a 10° threshold test within each 5-second data segment. The bearing standard deviations were then calculated from these values in 1-hour batches, and the hourly figures averaged, to produce the values shown. The bearing standard deviations for the wave-front test data range from .6 to .9 degrees, and thus are within the range of values found for the separated ionospheric modes as shown in Table 2. However, there is some scope for possible improvement if an orthogonal array were used to permit sorting by elevation angle.

TABLE 3

Standard Deviation of Bearings, Scan-by-Scan Wave-Front Test, Phase Threshold 10° rms

	Standard Deviation, Degrees	
	Day 167	Day 168
CW signal	.73	.60
SSB signal	.91	.76

6. CONCLUDING REMARKS

A theoretical analysis has been performed to delineate the general probability characteristics of the rms phase deviation across an antenna aperture in the presence of two and three-ray wave interference, when the ray amplitudes can be described by statistically-independent Rayleigh probability density functions. It is shown that in the worst case of equal average powers, the probability of observing an rms phase deviation of 25° or less across a large aperture is 0.2 if 3 rays are present, and 0.5 if only two rays are present.

The general probabilistic description of the behavior of wave-front nonlinearities has been confirmed by the results of two different experiments, and it has been shown that the bearing accuracy achievable by selection on the basis of a wavefront linearity threshold is comparable to that on single modes. It therefore seems likely that some further improvement in bearing accuracy could be achieved by making measurements on orthogonal arrays and applying a weighting procedure on the basis of elevation angle and possibly other factors.

Measurements have also shown that the time scale of changes in wave-front non-linearity can be significantly affected by the modulation imposed on the signal at the transmitter. In particular, the modulation can markedly shorten the waiting time between phase-linear events, which would otherwise be controlled by ionospheric fading with a period of the order of a second. The effect may be expected to be largest for signals which have significant amplitude modulation, with a bandwidth of the order of or greater than the reciprocal of the time delay between ionospheric modes. Thus the effect could best be exploited by a DF system which takes measurements on a similarly short time scale.

7. ACKNOWLEDGEMENT

I thank G.O. Venier who provided the data for Figure 13. This work was supported by the Department of National Defence of Canada.

8. REFERENCES

1. Anonymous, *Radio Direction Finder*. Wireless Eng. 13, 443 (1936).
2. Treharne, R.F., *Vertical Triangulation Using Skywaves*. Proc. IREE Aust., Vol. 28, p. 419 (November 1967).
3. Sherrill, W.M., *A Survey of Interferometry for Ionospheric Propagation Research*. Radio Science, Vol. 6 #5, 549, (May 1971).
4. Rice, D.W., G.O. Venier and G. Atkinson, *The Effect of Signal Modulation in the Application of a Wave-Front Linearity Test in HF Direction-Finding*. Proceedings of the 1978 NRL-ONR Symposium on the Effect of the Ionosphere on Space and Terrestrial Systems, Arlington, VA, January 24-26, 1978, paper 3-12.
5. Watterson, C.C., J.R. Juroshek, and W.D. Bensema, *Experimental Confirmation of an HF Channel Model*. IEEE Trans. Commun. Tech. COM-18, 792, (December 1970).
6. Gething, P.J.D., *Radio Direction-Finding and the Resolution of Multi-component Wave-Fields*. Peter Perigrines Ltd. (1978), p. 170.
7. Gething, P.J.D., *Radio Direction-Finding and the Resolution of Multi-component Wave-Fields*. Peter Perigrines Ltd. (1978), p. 75.
8. Davenport, W.B., *Probability and Random Processes*. McGraw-Hill Book Co., New York, 1979, Chapter 6.
9. Hayden, E.C., *Propagation Studies Using Direction-Finding Techniques*. J. Res. NBS-D, Radio Propagation, Vol. 65D, 197 (May - June 1961).
10. Rook, B.J., *Study of the Behavior and Stability of Phase Fronts on Short Time Scales*. Communications Research Centre, Report No. 1312, Ottawa, Canada., February 1978.
11. Rice, D.W., and E.L. Winacott, *A Sampling Array for HF Direction-Finding Research*. Communications Research Centre, Report No. 1310, Ottawa, Canada, (October 1977).

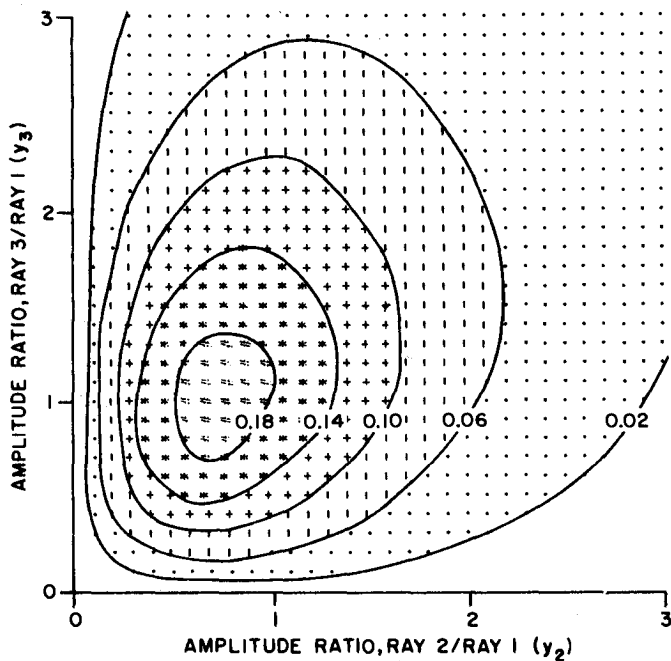


Figure 1. Contour plot of the 2-dimensional probability density function describing the amplitudes of ray 2 and ray 3 normalized by ray 1, when all three are subject to statistically-independent Rayleigh fading. The mean powers in rays 1, 2 and 3 are 1.0, 2.25, and 4.0 respectively.

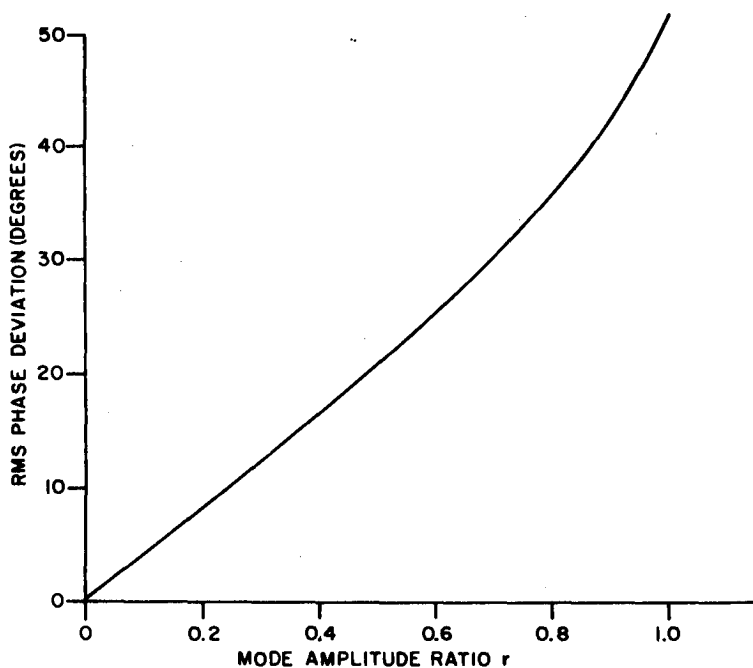


Figure 2. Root-mean-square phase deviation across an antenna aperture as a function of ray amplitude ratio r , for two rays incident upon the array.

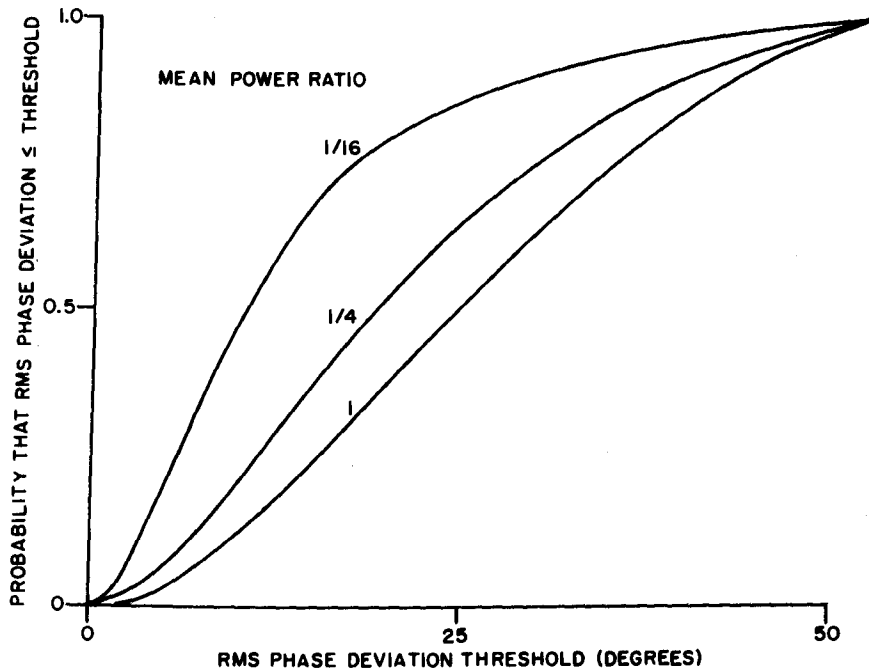


Figure 3. Cumulative probability distribution functions for the rms phase deviation σ_ϕ across an aperture, for two rays incident upon the array.

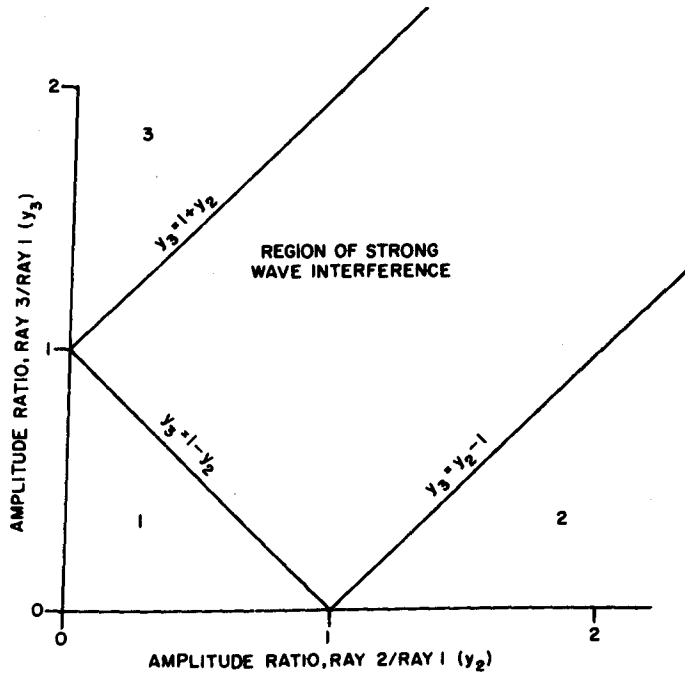


Figure 4. Boundaries separating strong and weak wave interference in the (y_2, y_3) plane. In region (1), ray 1 dominates, in region (2), ray 2 dominates, and in region (3), ray 3 dominates.

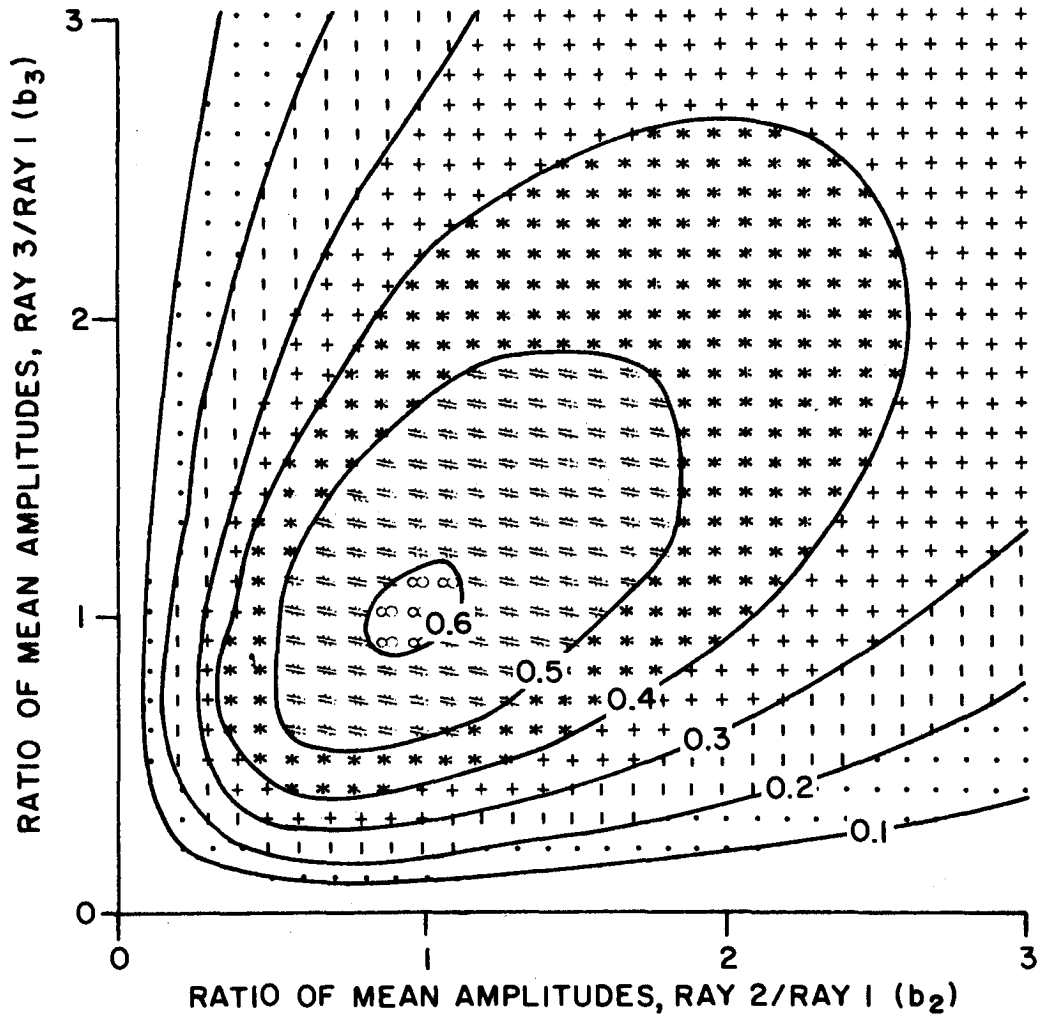


Figure 5. Contours of probability of strong wave interference when 3 rays are present, as a function of the mean powers in rays 2 and 3 normalized to ray 1. Strong wave interference is defined as the condition that the sum of the amplitudes of any two rays exceeds that of the third.

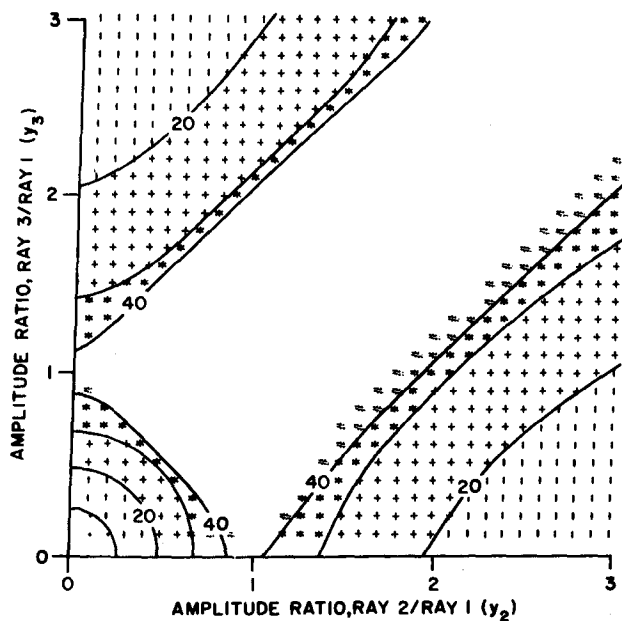


Figure 6(a). Contours of constant rms phase deviation σ_ϕ in degrees, as a function of the instantaneous amplitudes of rays 2 and 3, normalized to ray 1.

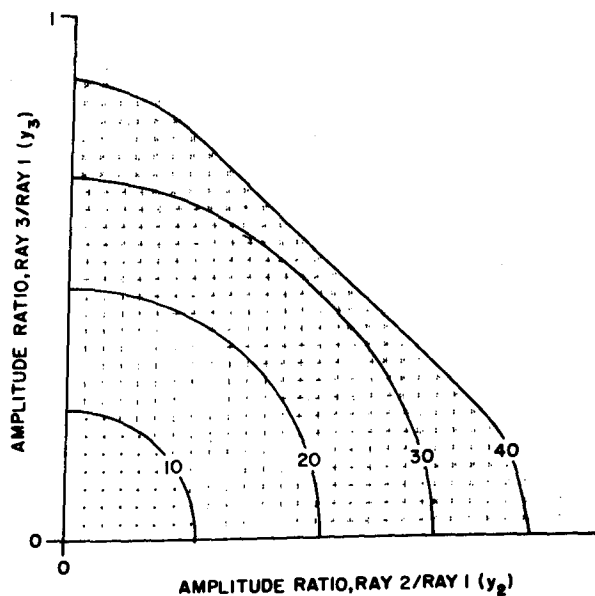


Figure 6(b). As in (a), except that the contours are more detailed and restricted to a region near the origin.

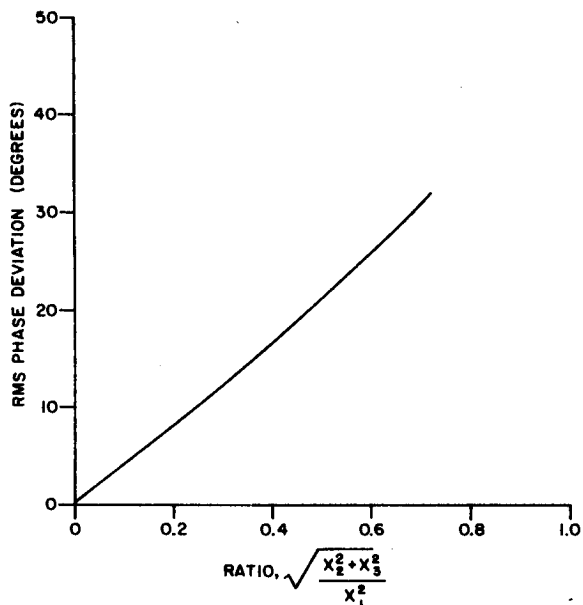


Figure 7. RMS phase deviation across an antenna aperture, for the case of 3 interfering rays. x_1^2 is the power associated with the dominant ray, while x_2^2 and x_3^2 are the powers associated with the weaker rays.

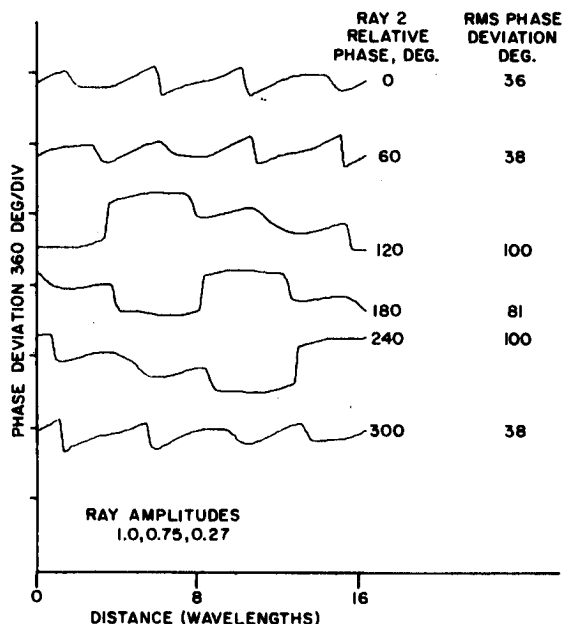


Figure 8. Computed phase fronts across a 16.6-wavelength aperture, near the region of transition from "strong" to "weak" wave interference. Ray amplitudes are 1.0, 0.75, and 0.27. Rays 1 and 3 are in-phase at the array origin, while the phase of ray 2 is varied in steps of 60° . Ray 1 is incident from array broadside, while rays 2 and 3 are displaced from broadside by 4 and 7 spatial cycles respectively.

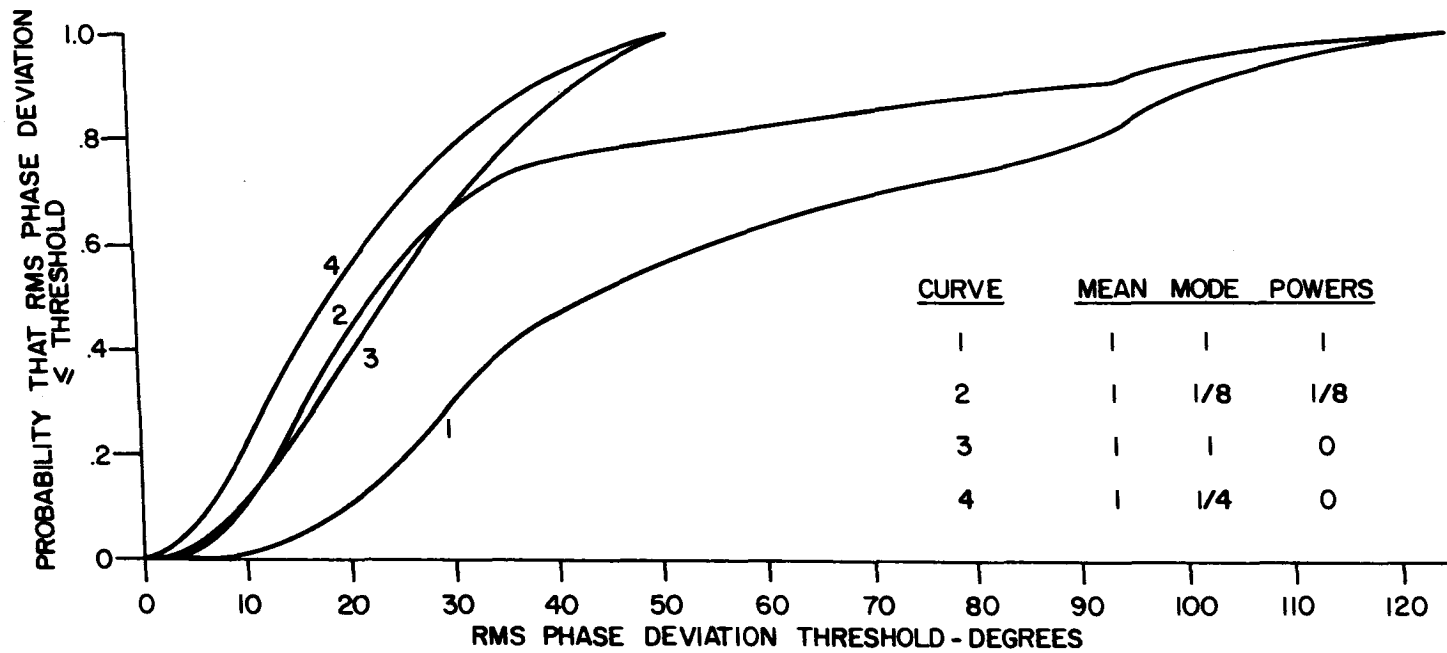


Figure 9. Cumulative probability distribution functions for the rms phase deviation σ_ϕ across an antenna aperture, for 3 rays incident upon the array (curves 1 and 2), and for 2 rays incident (curves 3 and 4).

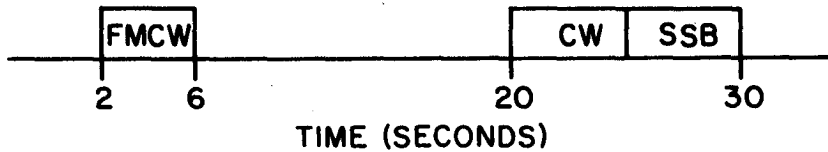


Figure 10. Transmitted signal timing sequence.

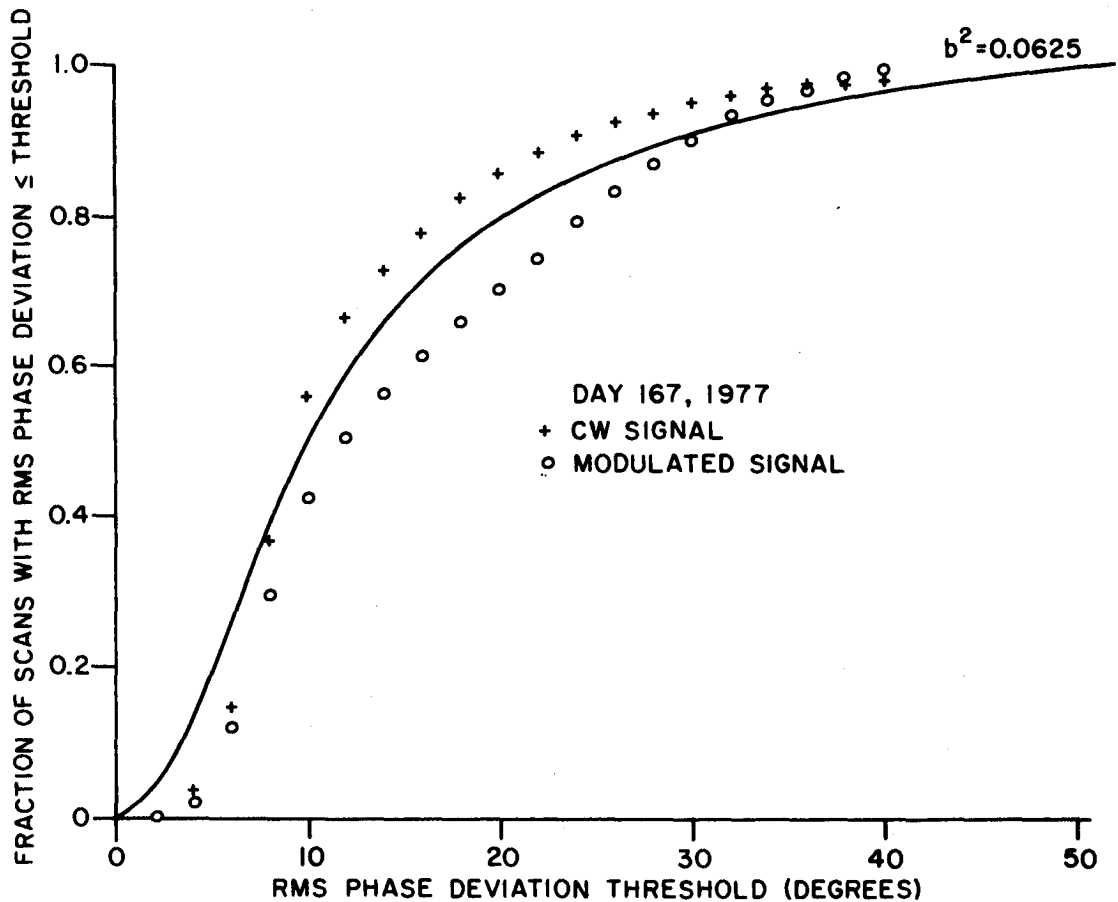


Figure 11. Cumulative distributions for the rms phase deviation as measured by the 6-element interferometer, for a CW signal (+) and a single-sideband signal (o). The solid curve is a theoretical result based on the assumption of 2 rays present, and with the ratio of mean powers b^2 adjusted to give a reasonable fit to the data. Day 167.

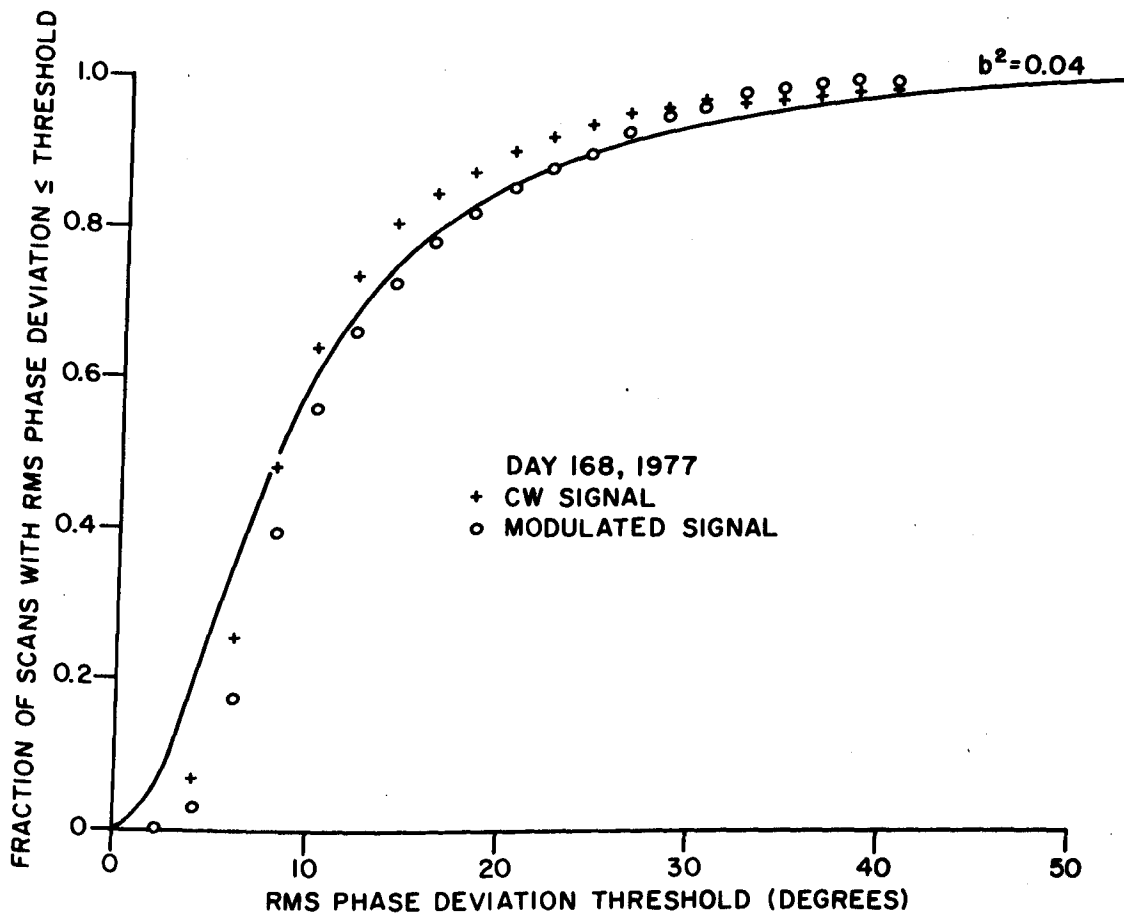


Figure 12. Cumulative distributions for the rms phase deviation as measured by the 6-element Interferometer, for a CW signal (+) and a single-sideband signal (o). The solid curve is a theoretical result based on the assumption of 2 rays present, and with the ratio of mean powers b^2 adjusted to give a reasonable fit to the data. Day 168.

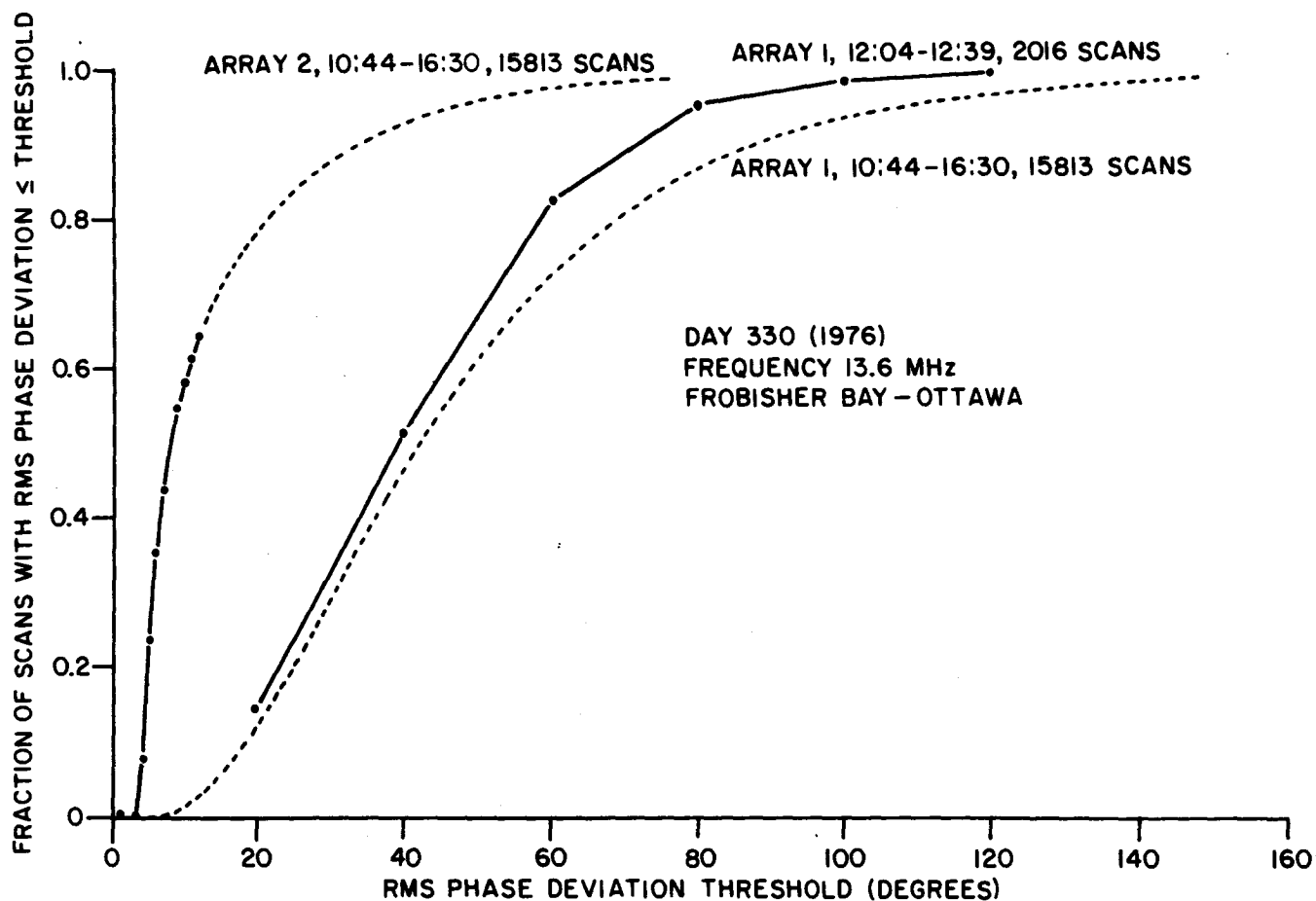
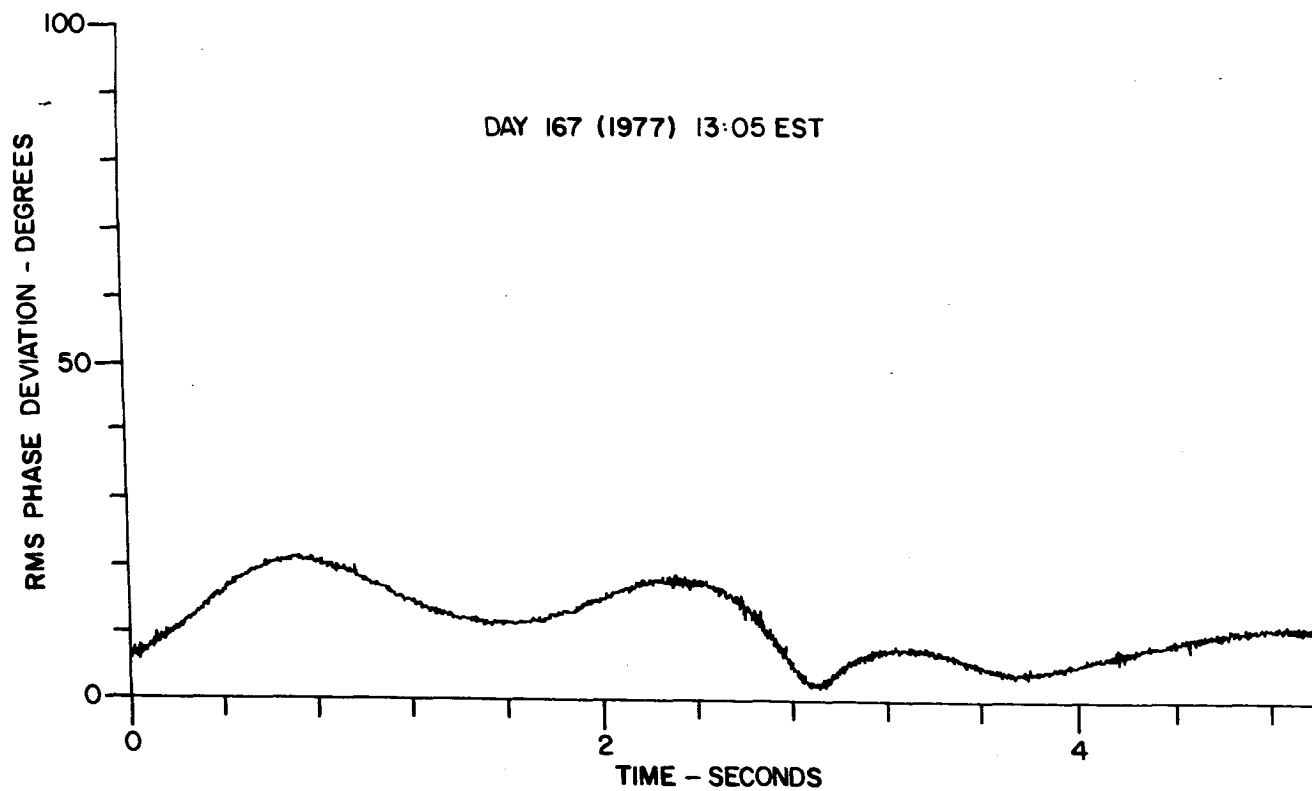


Figure 13. Cumulative distributions for the rms phase deviation as measured by an 1181-metre aperture (array 1), and a 236-metre aperture (array 2). CW signal; Frobisher Bay-Ottawa path.



*Figure 14. Measured rms phase deviation as a function of time for a CW transmitted signal.
Time of observation 13:05 EST, 16 June 1977.*

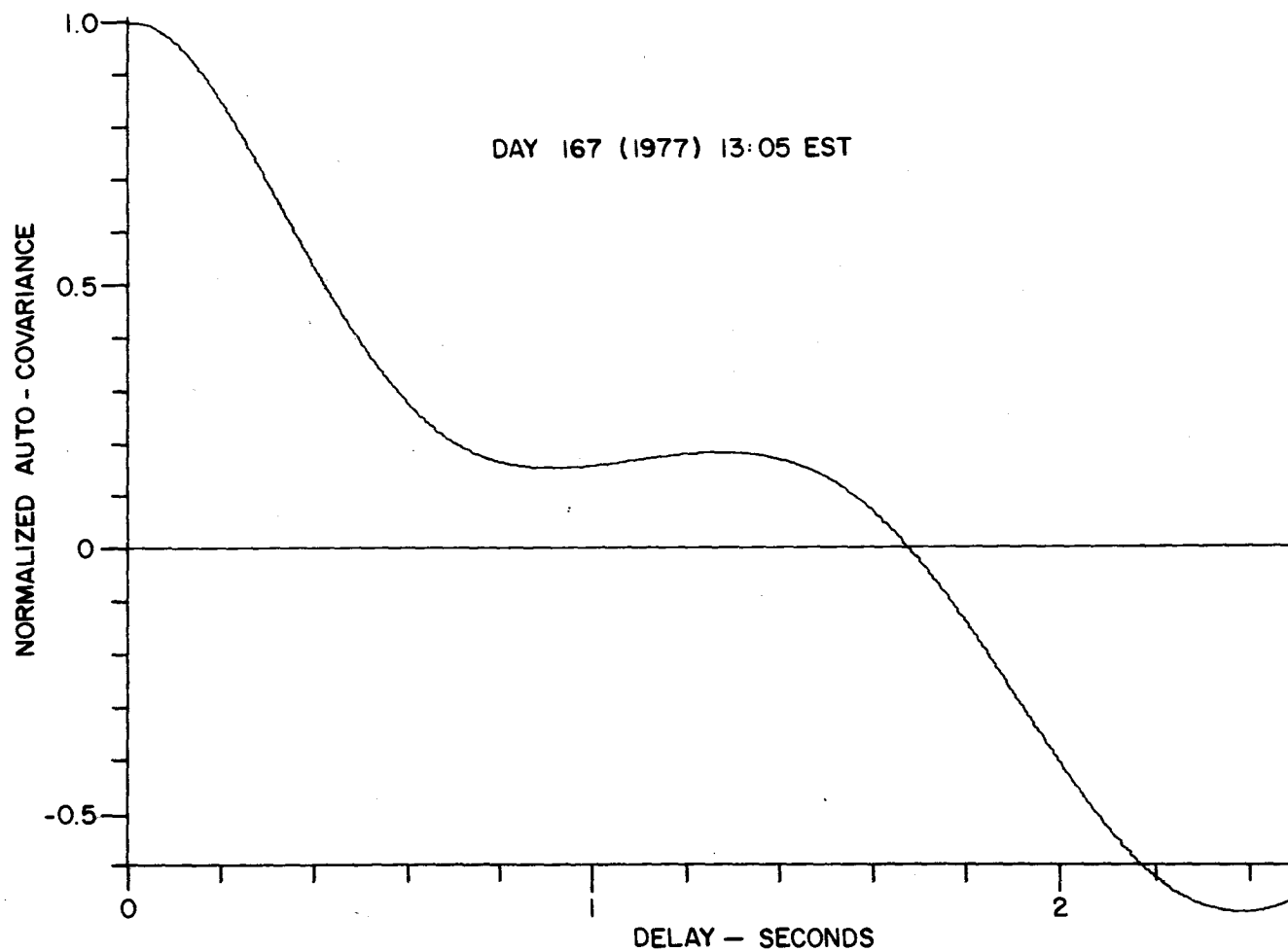
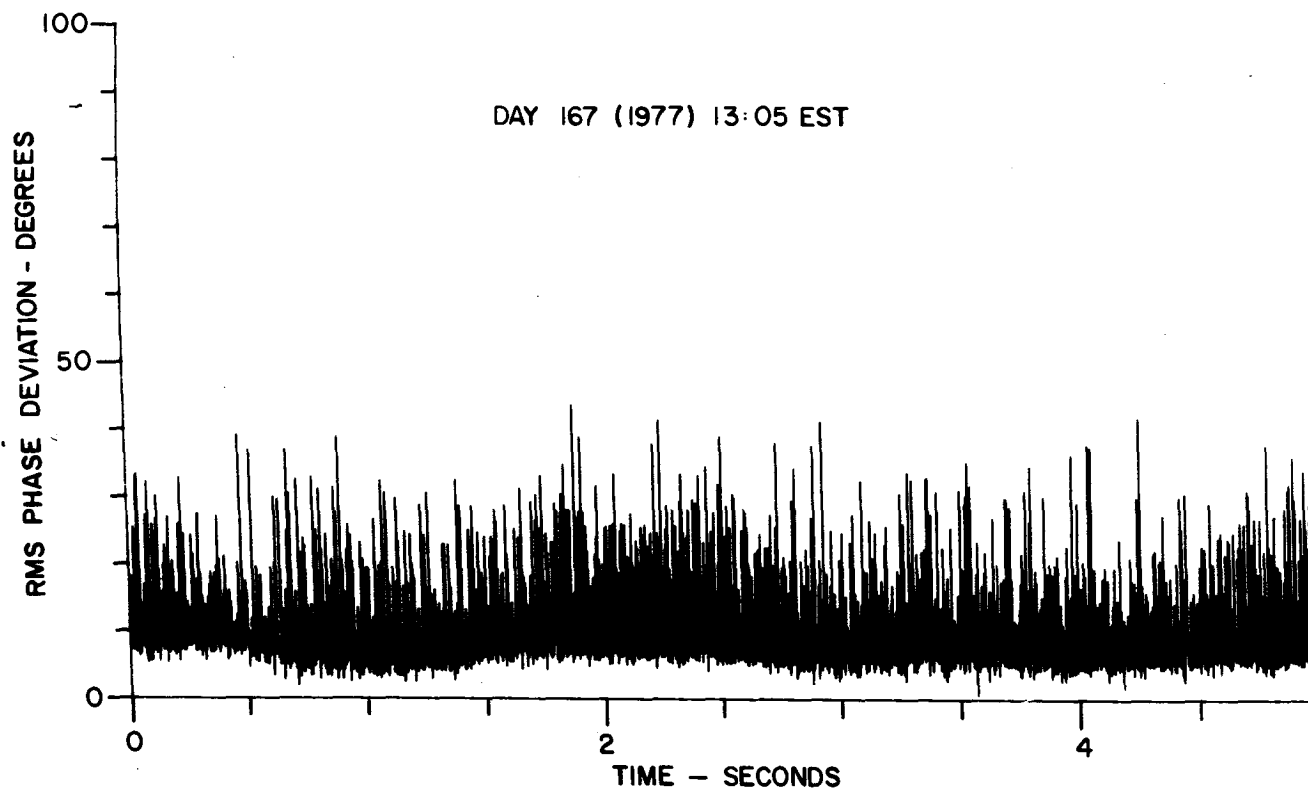


Figure 15. Normalized auto-covariance function for the data of Figure 14.



*Figure 16. Measured rms phase deviation as a function of time, for a SSB signal.
Time of observation 13:05 EST, 16 June 1977.*

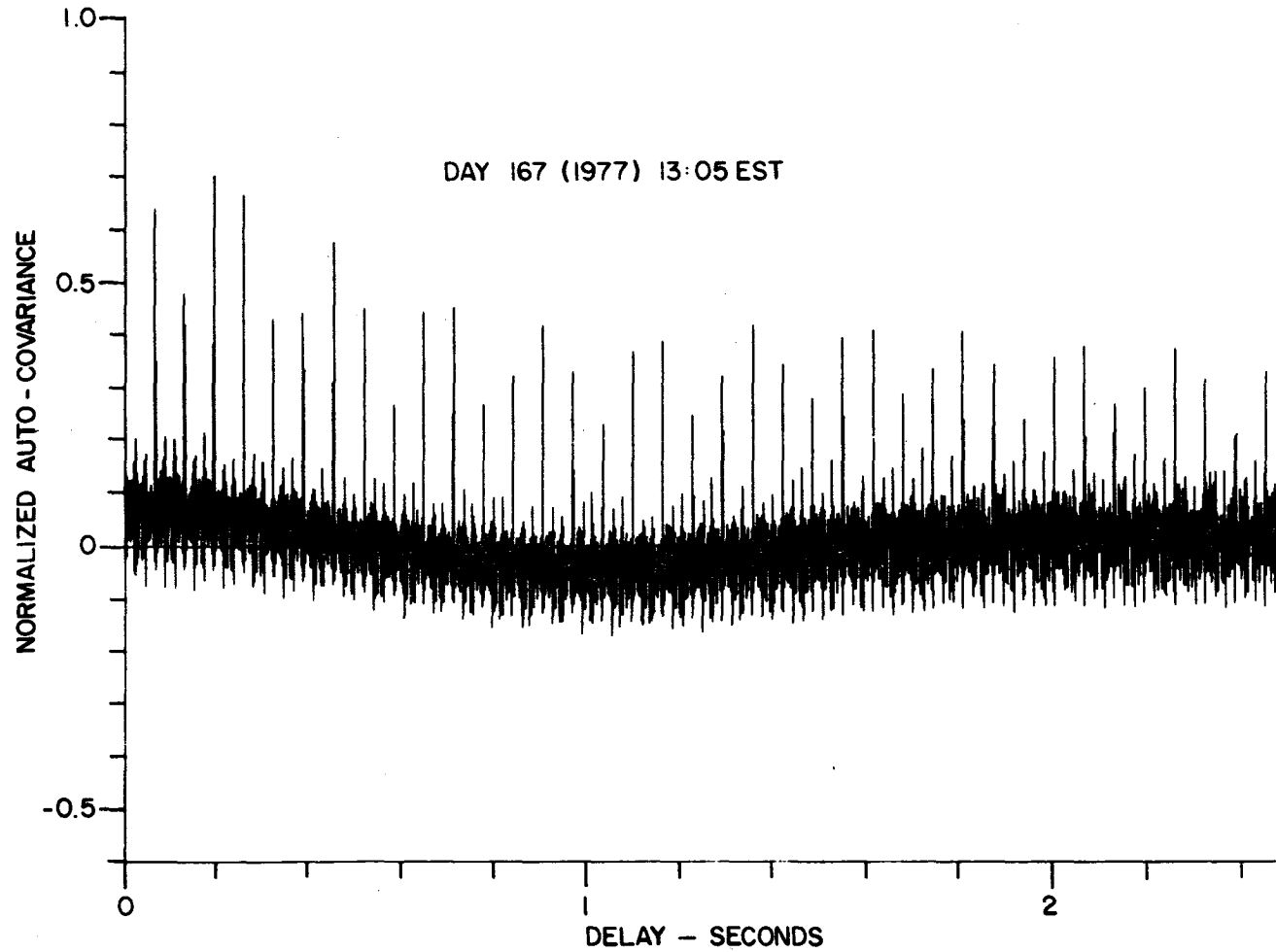


Figure 17. Normalized auto-covariance function for the data of Figure 16.

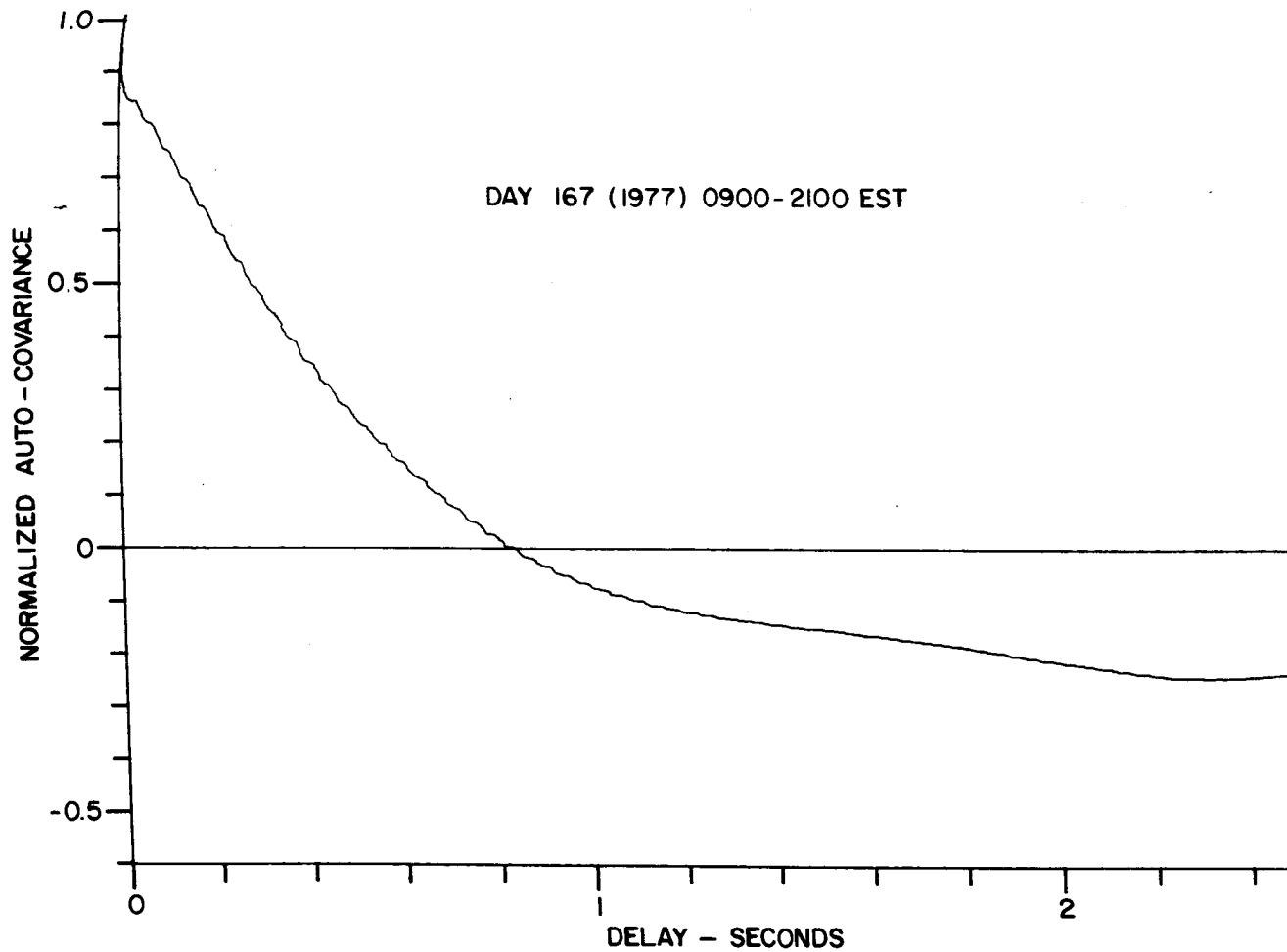


Figure 18. Normalized auto-covariance function for all CW data obtained over the 12-hour period from 0900-2100 EST, 16 June 1977.

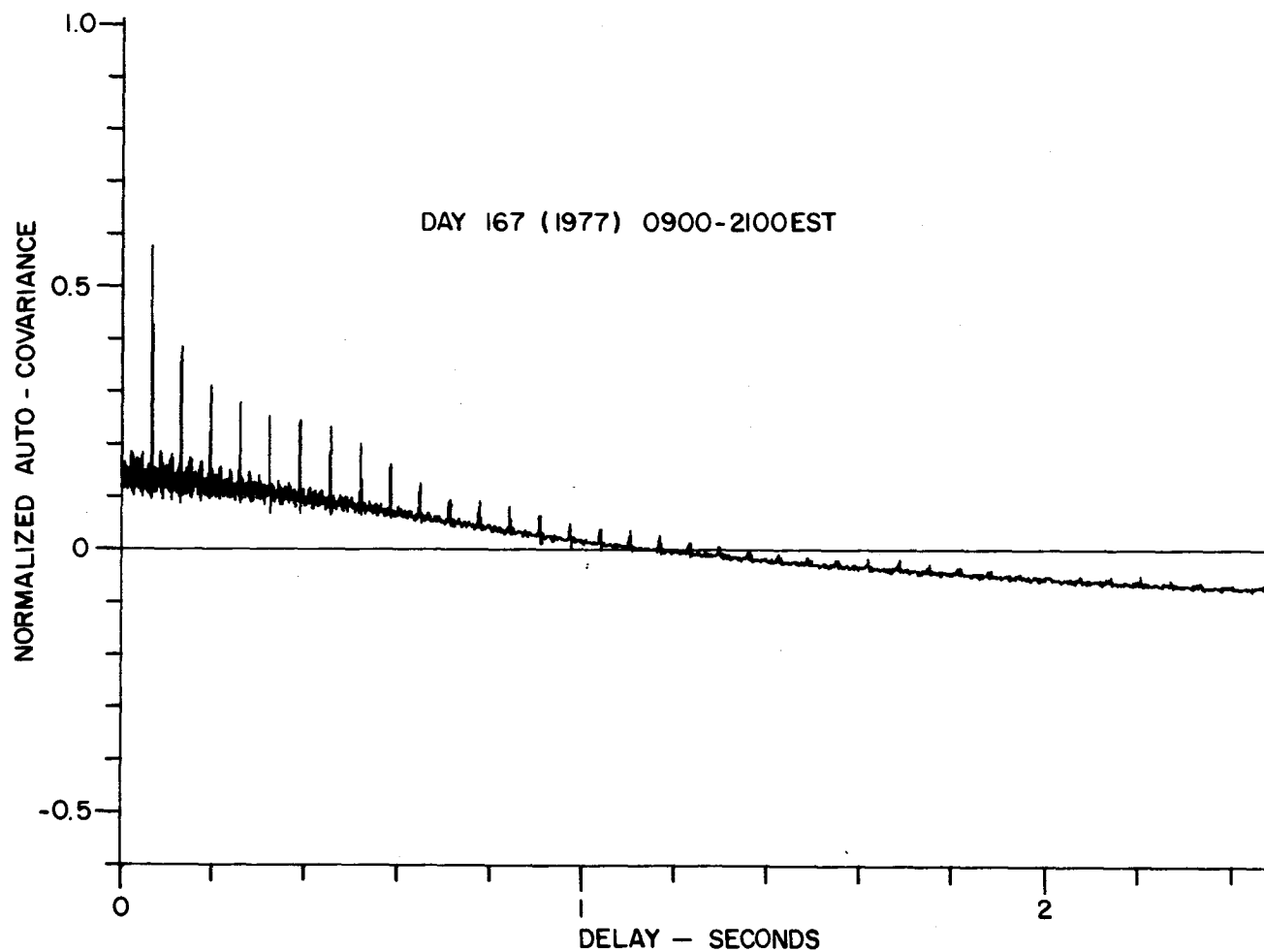


Figure 19. Normalized auto-covariance function for all SSB-signal data obtained over the 12-hour period from 0900-2100 EST, 16 June 1977.

APPENDIX A

Mathematical Details

In this Appendix we derive the principal results which are quoted in the main body of the report.

Probability Density Function for y_2, y_3

Equation (8) for the joint probability density function of variables y_1, y_2, y_3 is

$$f_{Y_1 Y_2 Y_3}(y_1, y_2, y_3) = \frac{y_1^5 y_2 y_3}{a_1^2 a_2^2 a_3^2} \exp - \left\{ \frac{y_1^2}{2a_1^2} + \frac{y_1^2 y_2^2}{2a_2^2} + \frac{y_1^2 y_3^2}{2a_3^2} \right\} \quad (A1)$$

and the joint probability density for variables y_2 and y_3 is obtained by integrating equation (A1) over y_1 ,

$$f_{Y_2 Y_3}(y_2, y_3) = \int_0^\infty f_{Y_1 Y_2 Y_3}(y_1, y_2, y_3) dy_1 \quad (A2)$$

$$= \frac{y_2 y_3}{a_1^2 a_2^2 a_3^2} \int_0^\infty y_1^5 \exp - \left\{ \frac{y_1^2}{2b^2} \right\} dy_1 \quad (A3)$$

$$\text{where } \frac{1}{b^2} = \frac{1}{a_1^2} + \frac{y_2^2}{a_2^2} + \frac{y_3^2}{a_3^2} \quad (A4)$$

Equation (A3) may be integrated by parts using

$$\int u dv = uv - \int v du \quad (A5)$$

with the substitutions

$$u = y_1^4, \quad dv = y_1 \exp - \left\{ \frac{y_1^2}{2b^2} \right\} dy_1$$

and hence

$$du = 4y_1^3 dy_1, \quad v = -b^2 \exp - \left\{ \frac{y_1^2}{2b^2} \right\}$$

(A6)

Then (A3) becomes

$$f_{Y_2 Y_3}(y_2, y_3) = \frac{y_2 y_3}{a_1^2 a_2^2 a_3^2} \left[-b^2 y_1^4 \exp - \left\{ \frac{y_1^2}{2b^2} \right\} \right]_0^\infty + 4b^2 \int_0^\infty y_1^3 \exp - \left\{ \frac{y_1^2}{2b^2} \right\} dy_1 \quad (A7)$$

The first term in the square brackets is zero at both limits, and the second term may again be integrated by parts, where

$$u = 4b^2 y_1^2, \quad dv = y_1 \exp - \left\{ \frac{y_1^2}{2b^2} \right\} dy_1$$

and hence

$$du = 8b^2 y_1 dy_1, \quad v = -b^2 \exp - \left\{ \frac{y_1^2}{2b^2} \right\}$$

(A8)

Hence (A7) becomes

$$f_{Y_2 Y_3}(y_2, y_3) = \frac{y_2 y_3}{a_1^2 a_2^2 a_3^2} \left[-4b^4 y_1^2 \exp - \left\{ \frac{y_1^2}{2b^2} \right\} \right]_0^\infty + 8b^4 \int_0^\infty y_1 \exp - \left\{ \frac{y_1^2}{2b^2} \right\} dy_1$$

$$= \frac{8y_2y_3b^4}{a_1^2a_2^2a_3^2} \int_0^\infty b^2 \exp - \left\{ \frac{y_1^2}{2b^2} \right\} d \left\{ \frac{y_1^2}{2b^2} \right\} \quad (A9)$$

or,

$$f_{Y_2Y_3}(y_2, y_3) = \frac{8 y_2 y_3 b^6}{a_1^2 a_2^2 a_3^2} \quad (A10)$$

Substituting (A4) into (A10), we have

$$f_{Y_2Y_3}(y_2, y_3) = \frac{8 y_2 y_3 a_1^4 a_2^4 a_3^4}{(a_2^2 a_3^2 + a_1^2 a_3^2 y_2^2 + a_1^2 a_2^2 y_3^2)^3} \quad (A11)$$

$$\text{Define } b_2^2 = a_2^2/a_1^2, \quad b_3^2 = a_3^2/a_1^2 \quad (A12)$$

Then (A11) can be put in the form

$$f_{Y_2Y_3}(y_2, y_3) = \frac{8(y_2/b_2^2)(y_3/b_3^2)}{[1 + (y_2/b_2^2)^2 + (y_3/b_3^2)^2]^3} \quad (A13)$$

which is equation (9).

Probability Density Function for y_2

To obtain the probability density function for variable y_2 alone, it is necessary to integrate equation (A13) over y_3 :

$$\begin{aligned} f_{Y_2}(y_2) &= \frac{8y_2}{b_2^2 b_3^2} \int_0^\infty \frac{y_3}{[1 + y_2^2/b_2^2 + y_3^2/b_3^2]^3} dy_3 \quad (A14) \\ &= \frac{4 y_2}{b_2^2 b_3^2} b_3^2 \left[1 + y_2^2/b_2^2 + y_3^2/b_3^2 \right]^{-2} \left[-\frac{1}{2} \right] \bigg|_0^\infty \end{aligned}$$

or

$$f_{Y_2}(y_2) = \frac{y_2^2}{b_2^2 [1 + y_2^2/b_2^2]^2} \quad (\text{A15})$$

which is equation (10).

Probability of Strong Interference

The integral of equation (9) over the interior region shown in Figure 4, yields the probability that the sum of the amplitudes of any two rays exceeds the third, a condition we define as "strong" wave interference.

Let $P[S]$ denote the probability of strong wave interference. Then

$$\begin{aligned} P[S] = & \int_{y_2=0}^1 \int_{y_3=1-y_2}^{1+y_2} f_{Y_2 Y_3}(y_2, y_3) dy_3 dy_2 \\ & + \int_{y_2=1}^{\infty} \int_{y_3=y_2-1}^{y_2+1} f_{Y_2 Y_3}(y_2, y_3) dy_3 dy_2 \end{aligned} \quad (\text{A16})$$

where $f_{Y_2 Y_3}(y_2, y_3)$ is given by equation (9). The inner integral in (A16) is the same as in (A14), except for the limits. Putting in the limits, and noting that the square of the lower limits $1 - y_2$ and $y_2 - 1$ are equal, (A16) becomes

$$\begin{aligned} P[S] = & \frac{2}{b_2^2} \int_0^{\infty} \left\{ \frac{y_2}{\left[1 + y_2^2/b_2^2 + \frac{(1 - y_2)^2}{b_3^2} \right]^2} - \frac{y_2}{\left[1 + y_2^2/b_2^2 + \frac{(1 + y_2)^2}{b_3^2} \right]^2} \right\} dy_2 \\ = & 2 \int_0^{\infty} \left\{ \frac{b_2^2 b_3^4 y_2}{[y_2^2 (b_2^2 + b_3^2) - 2b_2^2 y_2 + b_2^2 (1 + b_3^2)]^2} \right. \\ & \left. - \frac{b_2^2 b_3^4 y_2}{[y_2^2 (b_2^2 + b_3^2) + 2b_2^2 y_2 + b_2^2 (1 + b_3^2)]^2} \right\} dy_2 \end{aligned} \quad (\text{A17})$$

In the first integral in (A17), let

$$R_1 = (b_2^2 + b_3^2) y_2^2 - 2b_2^2 y_2 + b_2^2(1 + b_3^2) \quad (\text{A18})$$

and in the second integral let

$$R_2 = (b_2^2 + b_3^2) y_2^2 + 2b_2^2 y_2 + b_2^2(1 + b_3^2) \quad (\text{A19})$$

By completing the square in each case, (A18) becomes

$$R_1 = (b_2^2 + b_3^2) \left\{ \left(y_2 - \frac{b_2^2}{b_2^2 + b_3^2} \right)^2 + \left(\frac{b_2^2(1 + b_3^2)}{b_2^2 + b_3^2} - \frac{b_2^4}{(b_2^2 + b_3^2)^2} \right) \right\} \quad (\text{A20})$$

and (A19) becomes

$$R_2 = (b_2^2 + b_3^2) \left\{ \left(y_2 + \frac{b_2^2}{b_2^2 + b_3^2} \right)^2 + \left(\frac{b_2^2(1 + b_3^2)}{b_2^2 + b_3^2} - \frac{b_2^4}{(b_2^2 + b_3^2)^2} \right) \right\} \quad (\text{A21})$$

$$\left. \begin{array}{l} \text{Let } u_1 = y_2 - \frac{b_2^2}{b_2^2 + b_3^2} \\ \text{and } u_2 = y_2 + \frac{b_2^2}{b_2^2 + b_3^2} \end{array} \right\} \quad (\text{A22})$$

Also, let

$$B^2 = \frac{b_2^2 (1 + b_3^2)}{b_2^2 + b_3^2} - \frac{b_2^4}{(b_2^2 + b_3^2)^2} \quad (\text{A23})$$

which has the more convenient form

$$B^2 = \frac{b_2^2 b_3^2 (1 + b_2^2 + b_3^2)}{(b_2^2 + b_3^2)^2} \quad (\text{A24})$$

With the substitutions (A18) - (A24), (A17) becomes

$$P[S] = \frac{2 b_2^2 b_3^4}{(b_2^2 + b_3^2)^2} \int_{u_1 = -\frac{b_2^2}{b_2^2 + b_3^2}}^{\infty} \frac{u_1 + \frac{b_2^2}{b_2^2 + b_3^2}}{[u_1^2 + B^2]^2} du_1$$

$$- \frac{2 b_2^2 b_3^4}{(b_2^2 + b_3^2)^2} \int_{u_2 = \frac{b_2^2}{b_2^2 + b_3^2}}^{\infty} \frac{u_2 - \frac{b_2^2}{b_2^2 + b_3^2}}{[u_2^2 + B^2]^2} du_2 \quad (\text{A25})$$

Then

$$P[S] = \frac{b_2^2 b_3^4}{(b_2^2 + b_3^2)^2} \left\{ - \frac{1}{(u_1^2 + B^2)} \Big|_{u_1 = -\frac{b_2^2}{b_2^2 + b_3^2}}^{\infty} + \frac{1}{(u_2^2 + B^2)} \Big|_{u_2 = \frac{b_2^2}{b_2^2 + b_3^2}}^{\infty} \right\}$$

$$+ \frac{2 b_2^4 b_3^4}{(b_2^2 + b_3^2)^3} \left\{ \frac{u_1}{2B^2 (B^2 + u_1^2)} \Big|_{u_1 = \frac{-b_2^2}{b_2^2 + b_3^2}}^{\infty} + \frac{u_2}{2B^2 (B^2 + u_2^2)} \Big|_{u_2 = \frac{b_2^2}{b_2^2 + b_3^2}}^{\infty} \right\}$$

$$+ \frac{1}{2B^3} \left[\tan^{-1} \left(\frac{u_1}{B} \right) \Big|_{u_1 = \frac{-b_2^2}{b_2^2 + b_3^2}}^{\infty} + \tan^{-1} \left(\frac{u_2}{B} \right) \Big|_{u_2 = \frac{b_2^2}{b_2^2 + b_3^2}}^{\infty} \right]$$

Only the last pair of terms survive, thus

$$P[S] = \left[\frac{2b_2^4 b_3^4}{(b_2^2 + b_3^2)^3} \frac{(b_2^2 + b_3^2)^3}{2b_2^3 b_3^3 (1 + b_2^2 + b_3^2)^{3/2}} \right]$$

$$X \left[\pi - \tan^{-1} \left\{ \frac{-b_2^2}{B(b_2^2 + b_3^2)} \right\} - \tan^{-1} \left\{ \frac{b_2^2}{B(b_2^2 + b_3^2)} \right\} \right]$$

or

$$P[S] = \frac{\pi b_2 b_3}{[1 + b_2^2 + b_3^2]^{3/2}} \quad (A26)$$

which is equation (17).

Probability Density Function in Polar Co-ordinates

With the substitutions $y_2 = z \cos \theta$, $y_3 = z \sin \theta$, the integral of equation (9) over the first quadrant, out to radius z , is given by equation (18),

$$P[Z \leq z] = \int_{z=0}^z \int_{\theta=0}^{\frac{\pi}{2}} \frac{8 b_2^4 b_3^4 z^3 \sin \theta \cos \theta}{[b_2^2 b_3^2 + z^2 (b_3^2 \cos^2 \theta + b_2^2 \sin^2 \theta)]^3} d\theta dz \quad (A27)$$

$$\text{Now } \sin \theta \cos \theta d\theta = \frac{1}{2} d(\sin^2 \theta)$$

$$\left. \begin{aligned} & \text{and } b_2^2 \cos^2 \theta + b_3^2 \sin^2 \theta = b_3^2 + (b_2^2 - b_3^2) \sin^2 \theta \end{aligned} \right\} \quad (A28)$$

Putting these in (A27)

$$\begin{aligned}
 P[Z \leq z] &= \int_{z=0}^z \int_{\theta=0}^{\frac{\pi}{2}} \frac{4b_2^4 b_3^4 z^3 d(\sin^2 \theta)}{[b_2^2 b_3^2 + z^2 b_3^2 + z^2 (b_2^2 - b_3^2) \sin^2 \theta]^3} dz \\
 &= \frac{2b_2^4 b_3^4}{b_2^2 - b_3^2} \int_{z=0}^z \left\{ \frac{z}{[b_3^2 (b_2^2 + z^2)]^2} - \frac{z}{[b_2^2 (b_3^2 + z^2)]^2} \right\} dz
 \end{aligned}$$

or

$$P[Z \leq z] = 1 - \frac{b_2^2 b_3^2 + (b_2^2 + b_3^2) z^2}{(b_2^2 + z^2) (b_3^2 + z^2)} \quad (A29)$$

which is equation (19).

A P P E N D I X B

The Cumulative Probability Distribution for the RMS Phase Deviation in the Presence of Three Rays

The variation in space of the phase of a signal which is the summation of three rays can be calculated numerically by vector summation. For simplicity, we consider the three rays to be confined to a plane which also contains the linear antenna aperture. Additionally and without loss of generality, the first ray is assumed to have unit amplitude and to be incident from a direction perpendicular to the array. Then the net signal at distance d along the antenna array is

$$Ae^{j\phi} = 1 + y_2 e^{j\phi_2} + y_3 e^{j\phi_3} \quad (B1)$$

where $\phi_2 = \alpha_2 + \frac{2\pi d}{\lambda} \cos \theta_2$, $\phi_3 = \alpha_3 + \frac{2\pi d}{\lambda} \cos \theta_3$; α_2 and α_3 are arbitrary starting phases for rays 2 and 3 respectively at the array origin; θ_2 and θ_3 are the angles of incidence of rays 2 and 3, measured from the array axis.

The rms deviation σ_ϕ of the phase ϕ from the best-fit straight line is the parameter of interest. It is nearly independent of θ_2 and θ_3 provided, for total antenna aperture length L , $L/\lambda \cos \theta_2 \gg 1$, $L/\lambda \cos \theta_3 \gg 1$, and $|L/\lambda(\cos \theta_2 - \cos \theta_3)| \gg 1$, i.e., the rays are spread sufficiently in angle that the period of the interference patterns for the rays taken pair-wise, is much less than the size of the aperture. For the computations reported here, values of $L/\lambda \cos \theta_2 = 4$ and $L/\lambda \cos \theta_3 = 7.5$ were used.

The rms deviation σ_ϕ is a function of random variables α_2 , α_3 , y_2 and y_3 . The arbitrary starting phases α_2 and α_3 have no preferred values and hence have uniform probability densities over the interval $(0, 2\pi)$. The normalized amplitudes y_2 and y_3 have a joint probability density given by equation (A11) of Appendix A as

$$f_{Y_2 Y_3}(y_2, y_3) = \frac{8a_1^4 a_2^4 a_3^4 y_2 y_3}{(a_2^2 a_3^2 + a_1^2 a_3^2 y_2^2 + a_1^2 a_2^2 y_3^2)^3} \quad (B2)$$

where the a_i 's are proportional to the mean ray amplitudes. Thus given values of the variables α_2 , α_3 , y_2 , y_3 , and the parameters a_1 , a_2 , and a_3 , the

phase ϕ as a function of distance d along the array, and its rms deviation from a best-fit straight line, can be computed, along with the probability of the given set of variables occurring. The procedure can then be repeated over the range of all the parameters and the result accumulated appropriately to yield the cumulative probability distribution for σ_ϕ .

A difficulty arises because the probability density function for (y_2, y_3) , equation (B2), is defined on the semi-infinite space $(0 \leq y_2 < \infty, 0 \leq y_3 < \infty)$. In practice, the computer integration over (y_2, y_3) would have to be truncated. An alternative solution is however available.

It is equally valid to define the amplitude normalization in terms of any of the three amplitudes. Let the individual ray amplitudes be x_1 , x_2 and x_3 . The variables y_2 and y_3 were defined as

$$y_2 = \frac{x_2}{x_1}, \quad y_3 = \frac{x_3}{x_1} \quad (B3)$$

Define

$$u_1 = \frac{x_1}{x_2}, \quad u_3 = \frac{x_3}{x_2} \quad (B4)$$

and

$$w_1 = \frac{x_1}{x_3}, \quad w_2 = \frac{x_2}{x_3} \quad (B5)$$

Then in a method paralleling the derivation of equation (A11), other density functions in (u_1, u_3) and (w_1, w_2) coordinates may be obtained:

$$f_{U_1 U_3}(u_1, u_3) = \frac{8a_1^4 a_2^4 a_3^4 u_1 u_3}{\left(a_1^2 a_3^2 + a_2^2 a_3^2 u_1^2 + a_1^2 a_2^2 u_3^2\right)^3} \quad (B6)$$

and

$$f_{W_1 W_2}(w_1, w_2) = \frac{8a_1^4 a_2^4 a_3^4 w_1 w_2}{\left(a_1^2 a_2^2 + a_2^2 a_3^2 w_1^2 + a_1^2 a_3^2 w_2^2\right)^3} \quad (B7)$$

The u and w variables may also be expressed in terms of y_2 and y_3 , as follows:

$$u_1 = 1/y_2, \quad u_3 = y_3/y_2 \quad (B8)$$

and

$$w_1 = 1/y_3, \quad w_2 = y_2/y_3 \quad (B9)$$

Some consideration will show that the transformation (B8) maps the region in (y_2, y_3) space which is to the right of $y_2=1$ and below the diagonal $y_2=y_3$, to the unit square in (u_1, u_3) space, that is to the region $0 \leq u_1 \leq 1, 0 \leq u_3 \leq 1$. Similarly, transformation (B9) maps the region above $y_3=1$ and above the diagonal, to the unit square in (w_1, w_2) space. These transformations are illustrated in Figure B1. They provide a convenient method of numerically integrating over all probability space.

Based on this analysis, a computer program was written to compute the cumulative probability distribution for the rms phase deviation σ_ϕ . Figure B2 shows the main program flow. Results are plotted as curves 1 and 2 of Figure 9 of this report.

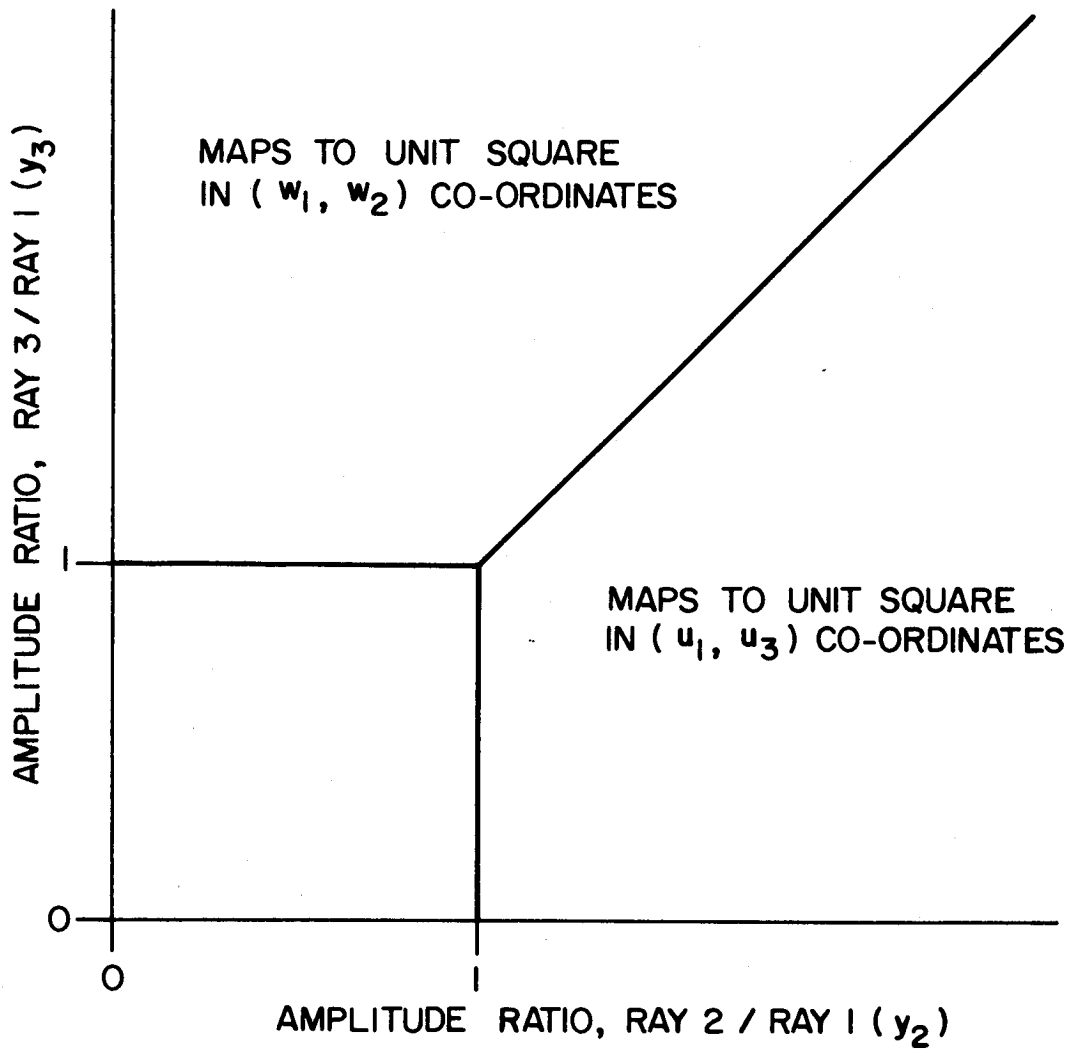


Figure B1. Mapping of (y_2, y_3) space to (w_1, w_2) and (u_1, u_3) coordinates.

DESCRIPTION	EQTN NO	STEP
FOR MODE AMPLITUDE RATIOS $y_2 = p, y_3 = q$; $p = 0.05$ to 0.95 at intervals of 0.1 ; $q = 0.05$ to 0.95 at intervals of 0.1		1
COMPUTE PROBABILITY DENSITIES $f_{Y_2 Y_3}(p, q), f_{U_1 U_3}(p, q), f_{W_1 W_2}(p, q)$	B2, B6, B7	2
TRANSFORM $u_1 = p, u_3 = q$ TO (y_2, y_3) CO-ORDINATES: $y_2 = \frac{1}{p}, y_3 = \frac{q}{p}$	B8	3
TRANSFORM $w_1 = p, w_2 = q$ TO (y_2, y_3) CO-ORDINATES: $y_2 = \frac{q}{p}, y_3 = \frac{1}{p}$	B9	4
FOR ALL α_2, α_3 IN RANGE $(0, 2\pi)$ AT INTERVALS OF $\frac{\pi}{6}$		5
FOR AMPLITUDE RATIOS $(p, q), \left(\frac{1}{p}, \frac{q}{p}\right), \left(\frac{q}{p}, \frac{1}{p}\right)$		6
COMPUTE NET SIGNAL AS A FUNCTION OF DISTANCE d BY VECTOR SUMMATION	B1	7
FIT STRAIGHT LINE TO THE COMPUTED PHASE VS d FUNCTION		8
COMPUTE RMS DEVIATION σ_ϕ FROM THE STRAIGHT LINE		9
FOR THE COMPUTED σ_ϕ , ADD ITS PROBABILITY OF OCCURRENCE (COMPUTED AT STEP 2), TO OCCURRENCE HISTOGRAM		10
CUMULATE OCCURRENCE HISTOGRAM TO OBTAIN CUMULATIVE PROBABILITY DISTRIBUTION FOR σ_ϕ		11

Figure B2. Program flow for computation of the cumulative probability distribution of the rms phase deviation across an antenna aperture, in the presence of three Rayleigh-fading signals.

RICE, D.W.
--HF direction finding by
wavefront testing.

TK
5102.5
C673e
#1333

DATE DUE
DATE DE RETOUR

SEP 29 1986

LOWE-MARTIN No. 1137

CRC LIBRARY/BIBLIOTHEQUE CRC
TK5102.5 C673e #1333 c. b

INDUSTRY CANADA / INDUSTRIE CANADA



209032

